JGP Journal of General Physiology

ARTICLE

Mechanotransduction by Membrane Proteins

C. elegans PEZO-1 is a mechanosensitive ion channel involved in food sensation

Jonathan R.M. Millet[1], Luis O. Romero[1,2], Jungsoo Lee[1], Briar Bell[1,2], and Valeria Vásquez[1a]

PIEZO channels are force sensors essential for physiological processes, including baroreception and proprioception. The *Caenorhabditis elegans* genome encodes an orthologue gene of the *Piezo* family, *pezo-1*, which is expressed in several tissues, including the pharynx. This myogenic pump is an essential component of the *C. elegans* alimentary canal, whose contraction and relaxation are modulated by mechanical stimulation elicited by food content. Whether *pezo-1* encodes a mechanosensitive ion channel and contributes to pharyngeal function remains unknown. Here, we leverage genome editing, genetics, microfluidics, and electropharyngeogram recording to establish that *pezo-1* is expressed in the pharynx, including in a proprioceptive-like neuron, and regulates pharyngeal function. Knockout (KO) and gain-of-function (GOF) mutants reveal that *pezo-1* is involved in fine-tuning pharyngeal pumping frequency, as well as sensing osmolarity and food mechanical properties. Using pressure-clamp experiments in primary *C. elegans* embryo cultures, we determine that *pezo-1* KO cells do not display mechanosensitive currents, whereas cells expressing wild-type or GOF PEZO-1 exhibit mechanosensitivity. Moreover, infecting the *Spodoptera frugiperda* cell line with a baculovirus containing the G-isoform of *pezo-1* (among the longest isoforms) demonstrates that *pezo-1* encodes a mechanosensitive channel. Our findings reveal that *pezo-1* is a mechanosensitive ion channel that regulates food sensation in worms.

Introduction

Mechanosensitive ion channels regulate several physiological processes including osmotic balance in bacteria (Kung et al., 2010; Martinac et al., 1987); turgor control in plants (Hamilton et al., 2015) and touch (Geffeney and Goodman, 2012; Yan et al., 2013; Ikeda et al., 2014; Maksimovic et al., 2014; Ranade et al., 2014; Woo et al., 2014; Chesler et al., 2016), pain (Murthy et al., 2018; Szczot et al., 2018), proprioception (Woo et al., 2015), hearing (Pan et al., 2018), lineage choice (Pathak et al., 2014), and blood pressure regulation in mammals (Retailleau et al., 2015; Wang et al., 2016; Rode et al., 2017; Zeng et al., 2018). These channels are ubiquitous, as they transduce mechanical stimuli into electrochemical signals in all kingdoms of life (Douguet and Honoré, 2019; Geffeney and Goodman, 2012; Kung et al., 2010). In 2010, the PIEZO1 and PIEZO2 channels were identified as essential components of distinct, mechanically activated cation channels in mammalian cells (Coste et al., 2010). Since then, many physiological roles have been assigned to these two ion channels (Parpaite and Coste, 2017).

Mammalian PIEZO channels have been associated with several hereditary pathophysiologies (Alper, 2017). *Piezo1* gain-of-function (GOF) mutations display slow channel inactivation, leading to an increase in cation permeability and subsequent red blood cell dehydration (Albuisson et al., 2013; Bae et al., 2013; Ma et al., 2018; Zarychanski et al., 2012). For instance, the human *Piezo1* hereditary mutation R2456H, located in the pore domain, decreases inactivation, while substitution by Lys slows inactivation even further (Bae et al., 2013). *Piezo1* global knockouts (KOs) are embryonically lethal in mice (Li et al., 2014; Ranade et al., 2014), and cell-specific KOs result in animals with severe defects (Ma et al., 2018; Wu et al., 2017a). Intriguingly, both *Piezo2* KO and GOF mutations are associated with joint contractures, skeletal abnormalities, and alterations in muscle tone (Chesler et al., 2016; Coste et al., 2013; Yamaguchi et al., 2019). GOF and loss-of-function (LOF) mutations are useful genetic tools for determining the contribution of PIEZO channels to mechanosensation in diverse physiological processes and in various animals.

The *Caenorhabditis elegans* genome encodes an orthologue of the PIEZO channel family, namely *pezo-1* (wormbase.org release

[1]Department of Physiology, College of Medicine, University of Tennessee Health Science Center, Memphis, TN; [2]Integrated Biomedical Sciences Graduate Program, College of Graduate Health Sciences, University of Tennessee Health Science Center, Memphis, TN.

Correspondence to Valeria Vásquez: vvasquez@uthsc.edu; J.R.M. Millet's present address is Institute of Neuroscience, Department of Biology, University of Oregon, Eugene, OR. This work is part of a special issue on mechanotransduction by membrane proteins.

WS280). Recently, Bai et al. (2020) showed that *pezo-1* is expressed in several tissues, including the pharynx. The worm's pharynx is a pumping organ that rhythmically couples muscle contraction and relaxation in a swallowing motion to pass food down to the animal's intestine (Keane and Avery, 2003). This swallowing motion stems from a constant low-frequency pumping, maintained by pharyngeal muscles, and bursts of high-frequency pumping from a dedicated pharyngeal nervous system (Avery and Horvitz, 1989; Lee et al., 2017; Raizen et al., 1995; Trojanowski et al., 2016). In mammals, the swallowing reflex is initiated when pressure receptors in the pharynx walls are stimulated by food or liquids, but the identity of the receptors that directly evoke this mechanical response remain to be identified (Tsujimura et al., 2019). Interestingly, the *Drosophila melanogaster* PIEZO orthologue is a mechanosensitive ion channel (Kim et al., 2012) required for feeding and is also important for avoiding food overconsumption (Min et al., 2021; Wang et al., 2020). To date, whether *pezo-1* encodes for a mechanosensitive ion channel or regulates worm pharyngeal activity has yet to be determined.

Here, we found a strong and diverse expression of the *pezo-1* gene in pharyngeal tissues by imaging a *pezo-1::GFP* transgenic reporter strain. By leveraging genetic dissection, electrophysiological measurements, and behavior analyses, we also established that PEZO-1 is required for proper low-frequency electrical activity and pumping behavior. Analyses of *pezo-1* KO and GOF mutants demonstrated that decreasing or increasing PEZO-1 function up-regulates pharyngeal parameters. Likewise, mutants display distinct pharyngeal activities triggered by the neurotransmitter serotonin or with various buffer osmolarities. Using elongated bacteria as a food source, we demonstrated that *pezo-1* KO decreases pharyngeal pumping frequency, whereas a GOF mutant features increased frequency. Finally, electrophysiological recordings of *pezo-1*–expressing cells from *C. elegans* embryo cultures and the *Spodoptera frugiperda* (Sf9) cell line demonstrate that *pezo-1* encodes a mechanosensitive ion channel. Altogether, our results reveal that PEZO-1 is a mechanosensitive ion channel involved in a novel biological function, regulating pharyngeal pumping and food sensation.

Materials and methods

Strains and maintenance

Worms were propagated as previously described (Brenner, 1974). N2 (var. Bristol) is referred to as WT throughout the paper. The following strains were used: VVR3 *unc119(ed3)III;decEx1(pRedFlpHgr)(C10C5.1[20789]::S0001_pR6K_Amp_2xTY1ce_EGFP_FRT_rpsl_neo_FRT_3xFlag)dFRT::unc-119-Nat*, COP1553 (KO, 6,616-bp deletion) *pezo-1 (knu508) IV*, COP1524 (GOF: R2373K) *pezo-1 (knu490) IV*, LX960 *lin-15B&lin-15A(n765) X*; *vsIs97 [tph-1p::DsRed2 + lin-15(+)]*, DA572 *eat-4(ad572) III*, and DA1051 *avr-15(ad1051) V*. Transgenic strain VVR3 was obtained by microinjecting a fosmid construct (from the TransgeneOme Project) into a *unc-119(ed3)* strain (InVivo Biosystems). COP1553 and COP1524 were obtained using the CRISPR-Cas9 method (InVivo Biosystems). Transgenic worm VVR3, expressing GFP under the control of *Ppezo-1::GFP*, was crossed with *pezo-1* mutants COP1553 and COP1524 to obtain VVR69 and VVR70, respectively. LX960 was kindly provided by Dr. Kevin Collins (University of Miami, Miami, FL).

Genomic DNA PCR

PCR was performed with worm lysates of N2 and COP1553. Phusion High-Fidelity DNA Polymerase (Thermo Fisher Scientific) was used to amplify *pezo-1* DNA fragments. Primer sequences are as follows: F1, 5′-GACGACCAACTGCCTACAT-3′; F2, 5′-TGCTGTAAATTAGCACTCGGGT-3′; and R1, 5′-TGTACCGTA ATCCAGAAACGCA-3′.

RNA isolation and RT-PCR

Cultured worms were washed with M9 buffer (86 mM NaCl, 42 mM Na_2HPO_4, 22 mM KH_2PO_4, and 1 mM $MgSO_4$) and collected into 15-ml Falcon tubes. Trizol was added to pelleted worms, and RNA was isolated using the freeze-cracking method as previously described (Van Gilst et al., 2005). Isolated total RNA was purified using the RNAeasy kit (Qiagen). The SuperScript III One-Step RT-PCR system with Platinum Taq DNA Polymerase was used for RT-PCR, following the manufacturer's protocol (Invitrogen). Primers were designed based on the *pezo-1* sequences comprising the deletion regions of the *knu508* allele of the COP1553 mutant: F3, 5′-GCAACGTCACCAAGAAGAGCAG-3′, and R2, 5′-GCATTCAATAGTCTCGTTGCTG-3′.

Imaging

Worms were individually selected and dropped into 15 µl of M9 buffer and then paralyzed on a glass slide with 2% agarose pads containing 150 mM 2,3-butanedione monoxime. Bright-field and fluorescence imaging were performed on a Zeiss 710 Confocal microscope using a 20× or 40× objective. Images were processed using Fiji ImageJ (Schindelin et al., 2012) to enhance contrast and convert to an appropriate format.

Worm synchronization

For all pharyngeal pumping assays, worms were synchronized by placing young adults onto fresh nematode growth media (NGM) plates seeded with OP50 (*Escherichia coli* strain) and left to lay eggs for 2 h at 20°C. Adults were removed, and the plates were incubated at 20°C for 3 d.

Pharyngeal pumping

Serotonin profile

A serotonin aliquot (InVivo Biosystems) was diluted in M9 Buffer before experiments and discarded after 3 h. 42 synchronized worms were picked and transferred to 200 µl of M9 Buffer supplemented with 2, 5, 10, or 20 mM serotonin and incubated at 20°C for 30 min before loading onto a microfluidic chip (SC40, The ScreenChip System; InVivo Biosystems).

Control E. coli *assay*

OP50 was grown in liquid Luria-Bertani (LB) medium under sterile conditions at 37°C and diluted to OD 1.0. Bacterial cultures were stored at 4°C for up to 1 wk.

Spaghetti-like E. coli *assay*

The day before the experiment, OP50 colonies were picked from a fresh LB plate and incubated in 2 ml of LB overnight. The

following day, 0.5 ml of this culture was used to inoculate 1.5 ml of LB medium and incubated until growth was exponential, which was verified by optical density (OD 0.5). Cephalexin (Alfa Aesar) was added to a final concentration of 60 µg/ml, and the culture was incubated for 2 h. Spaghetti-like OP50 were verified under a microscope and washed three times using 2 ml of M9 buffer, followed by centrifugation at 400 *g* to gently pellet the elongated bacteria.

Pharyngeal recordings and analyses

Worms were loaded one by one into the microfluidic chip recording channel and left to adjust for 1 min before recording. All recordings were 2 min long. Records were analyzed using NemAnalysis software (InVivo Biosystems) with the brute force algorithm turned off. Parameters were adjusted for each record to include the maximum number of clearly identifiable pharyngeal pumps. Results were exported from the software in sheet form, and parameters were plotted and statistically analyzed using Matlab R2019a (MathWorks). Matlab analysis code is available at: https://github.com/JonathanMillet/Pharyngeal_Pumping_Analysis_Script_JM2021.git.

Development assay

Young adults were allowed to lay eggs on NGM plates seeded with control or spaghetti-like bacteria for 2 h. Spaghetti-like bacteria were cultured as described above. Animals (10–20 worms) were removed from plates after 2 h, and the number of eggs laid was counted. After 3 d of incubation, animals that reached adulthood were counted in each trial, and results were compared across four trials.

Food ingestion assay

A drop of fresh culture containing control or spaghetti-like bacteria with 2 µM DiI dye (CAS 41085-99-8; Sigma-Aldrich) was placed on an NGM agar plate. Young adults were fed bacteria with DiI for 30 min. Next, worms were transferred onto OP50-seeded NGM without dye for 5 min (Vidal-Gadea et al., 2012). Finally, animals were placed on a thin-layered 2,3-butanedione monoxime–agarose plate for imaging under a Nikon SMZ18 stereomicroscope. Food occupation in the digestive tract was detected by fluorescence.

Primary culture of *C. elegans* embryo cells

C. elegans embryonic cells were generated as previously described (Strange et al., 2007). Worms were grown on 10-cm enriched peptone plates with NA22 *E. coli*. NA22 bacteria grow in very thick layers that provide an abundant food source for large quantities of worms. Synchronized gravid hermaphrodites were bleached to release eggs and washed with sterile egg buffer (118 mM NaCl, 48 mM KCl, 2 mM $CaCl_2$, 2 mM $MgCl_2$, and 25 mM HEPES, pH 7.3, 340 mOsm, adjusted with sucrose). The isolated eggs were separated from debris by centrifugation in a 30% sucrose solution. Chitinase (1 U/ml; Sigma-Aldrich) digestion was performed to remove eggshells. The embryo cells were dissociated by pipetting and filtered through a sterile 5-µm Durapore filter (Millipore). The cells were plated on glass coverslips coated with a peanut lectin solution (0.5 mg/ml; Sigma-Aldrich) and cultured in L15 medium (Gibco) supplemented with 50 U/ml penicillin, 50 µg/ml streptomycin, and 10% FBS (Invitrogen) for 72–96 h.

Expression of *pezo-1* in Sf9 insect cells

To express *pezo-1* in Sf9 cells, we produced recombinant baculoviruses, according to the manufacturer's instructions (Bac-to-Bac expression system; Invitrogen). To generate this baculovirus, we used a pFastBac construct (Epoch Life Science) containing an 8× histidine–maltose binding protein tag and a synthesized *pezo-1* isoform G nucleotide sequence (one of the longest isoforms according to RNA sequencing; wormbase.org release WS280). For expression of *pezo-1* R2373K, the construct contained an 8× histidine–maltose binding protein tag and a synthesized *pezo-1* isoform G with the R2373K point mutation. We infected Sf9 cells with either *pezo-1* baculovirus for 48 h. Infected cells were plated on glass coverslips coated with a peanut lectin solution (1 mg/ml; Sigma-Aldrich) for patch-clamp experiments.

Electrophysiology and mechanical stimulation

Primary cultured embryo cells labeled with *Ppezo-1::GFP* from strains VVR3, VVR69, or VVR70 were recorded in the cell-attached configuration of the patch-clamp technique. Control and infected Sf9 insect cells were recorded in the whole-cell or inside-out patch-clamp configurations. For on-cell recordings, the bath solution contained 140 mM KCl, 6 mM NaCl, 2 mM $CaCl_2$, 1 mM $MgCl_2$, 10 mM glucose, and 10 mM HEPES, pH 7.4; 340 mOsm, adjusted with sucrose. The pipette solution contained 140 mM NaCl, 6 mM KCl, 2 mM $CaCl_2$, 1 mM $MgCl_2$, 10 mM glucose, and 10 mM HEPES, pH 7.3; 330 mOsm, adjusted with sucrose. Cells were mechanically stimulated with negative pressure applied through the patch pipette using a High-Speed Pressure Clamp (ALA Scientific) controlled with a MultiClamp 700B amplifier through Clampex (Molecular Devices). Cell-attached patches were probed using a square-pulse protocol consisting of −10-mmHg incremental pressure steps, each lasting 1 s, in 10-s intervals. Cells with giga-seals that did not withstand at least six consecutive steps of mechanical stimulation were excluded from analyses. I_{steady} was defined as the maximal current in the steady state. Deactivation was compared by determining the percentage of I_{steady} remaining 100 ms after removal of the mechanical stimuli.

For whole-cell recordings, the bath solution contained 140 mM NaCl, 6 mM KCl, 2 mM $CaCl_2$, 1 mM $MgCl_2$, 10 mM glucose, and 10 mM HEPES, pH 7.4. The pipette solution contained 140 mM CsCl, 5 mM EGTA, 1 mM $CaCl_2$, 1 mM $MgCl_2$, and 10 mM HEPES, pH 7.2. For indentation assays, Sf9 cells were mechanically stimulated with a heat-polished blunt glass pipette (3–4 µm) driven by a piezo servo controller (E625; Physik Instrumente). The blunt pipette was mounted on a micromanipulator at an ∼45° angle and positioned 3–4 µm above the cells without indenting them. Displacement measurements were obtained with a square-pulse protocol consisting of 1-µm incremental indentation steps, each lasting 200 ms, with a 2-ms ramp in 10-s intervals. Recordings with leak currents >200 pA and with access resistance >10 MΩ, as well as cells with giga-seals that did not withstand at least five consecutive steps of mechanical stimulation, were excluded from analyses. For

inside-out recordings, symmetrical conditions were established with a solution containing 140 mM CsCl, 5 mM EGTA, 1 mM $CaCl_2$, 1 mM $MgCl_2$, and 10 mM HEPES, pH 7.2, and mechanical stimulation was performed identically to on-cell recordings. Pipettes were made from borosilicate glass (Sutter Instruments) and were fire-polished before use until a resistance between 3 and 4 MΩ was reached. Currents were recorded at a constant voltage (−60 mV, unless otherwise noted), sampled at 20 kHz, and low-pass filtered at 2 kHz using a MultiClamp 700B amplifier and Clampex (Molecular Devices). Leak currents before mechanical stimulation were subtracted offline from the current traces.

Data and fits were plotted using OriginPro (OriginLab). Sigmoidal fit was done with the following Boltzmann equation:

$$f_{(x)} = A_2 + \frac{A_1 - A_2}{1 + e^{(X-X_o)/dX}}, \quad (1)$$

where A_2 = final value, A_1 = initial value; X_o = center, and dX = time constant.

The time constant of inactivation τ was obtained by fitting a single exponential function, Eq. 2, between the peak value of the current and the end of the stimulus:

$$f_{(t)} = \sum_{i=1}^{n} A_i * e^{-t/\tau_i} + C, \quad (2)$$

where A = amplitude, τ = time constant, and the constant y-offset C for each component i.

Data and statistical analyses

Data and statistical analyses were performed using DataGraph 4.6.1, Matlab R2019a (MathWorks), and GraphPad Instat 3 software. Statistical methods and sample numbers are detailed in the corresponding figure legends. No technical replicates were included in the analyses.

Online supplemental material

Fig. S1 shows *pezo-1::GFP* expression at different developmental stages and in various tissues in *C. elegans*. Fig. S2 shows the molecular details of the *pezo*-1 KO strain (COP1553; *pezo-1 (knu508) IV*). Fig. S3 shows the pharyngeal pumping frequencies of WT, *pezo-1* KO, and R2373K challenged with 2 mM serotonin or fed with control *E. coli*. Fig. S4 shows the differences between control and spaghetti-like *E.* coli and their effect in WT and *pezo-1* mutants' physiological traits (feeding, development, and pharyngeal pumping frequency). Fig. S5 shows the GFP intensity across the worm strains used to generate embryo cultures for patch-clamp experiments. Fig. S6 shows single-channel trace recordings and current–voltage relationships of WT cells expressing *pezo-1::GFP* in the cell-attached configuration. Fig. S7 shows representative single-channel trace recordings of pressure-evoked currents from *pezo-1::GFP* cells expressing *pezo-1* WT and R2373K. Fig. S8 shows the current densities evoked with displacement of naive and *pezo-1*–infected Sf9 cells. Fig. S9 shows representative single-channel trace recordings of pressure-evoked currents from Sf9 cells expressing *pezo-1* WT and R2373K.

Results

pezo-1 is expressed in a wide variety of cells in the worm pharynx

To determine the expression of *pezo-1* in *C. elegans*, we used a fluorescent translational reporter made by the TransgeneOme Project (Hasse et al., 2016). This fosmid construct contains *pezo-1* native cis-regulatory elements, including introns, up to exon 17 and 3′ untranslated region (UTR) sequences linked in-frame to GFP (Fig. 1 A). The position of GFP with respect to the remainder of the gene creates an unnatural truncated version of the PEZO-1 protein. Hence, it likely expresses a nonfunctional protein that excludes 16 exons, which contain most of the *pezo-1* sequence (including the pore domain). GFP signals are present in multiple cells at all developmental stages (Fig. S1, A and B). Furthermore, it does not appear to be mosaic, as similar expression patterns were observed in at least three independent transgenic lines. We imaged *pezo-1::GFP* worms at various focal planes to identify the different cells expressing GFP based on their morphological features (i.e., cell-body position, neurites extension and position along the body, and branching; Fig. 1, B–G). The strongest GFP signals that we identified came from the pharyngeal gland cells (Fig. 1 B, bright and fluorescence fields). These cells are composed of five cell bodies (two ventral g1s, one dorsal g1, and two ventral g2s) located inside the pharynx terminal bulb and three anterior cytoplasmic projections: two short projections that are superposed, ending in the metacorpus, and a long projection reaching the end of the pm3 muscle. These cells are proposed to be involved in digestion (Albertson and Thomson, 1976; Ohmachi et al., 1999), lubrication of the pharynx (Smit et al., 2008), generation and molting of the cuticle (Höflich et al., 2004; Singh and Sulston, 1978), and resistance to pathogenic bacteria (Höflich et al., 2004). Additionally, we visualized *pezo-1::GFP* in a series of cells surrounding the muscle of the corpus and the isthmus (Fig. 1 C; Albertson and Thomson, 1976). We also recognized the arcade cells as putative *pezo-1*–expressing cells, according to their morphology and location (Fig. 1, C and E). Arcade cells and the pharyngeal epithelium form the buccal cavity and connect the digestive tract to the outside (Altun and Hall, 2009). We also observed many other anterior cells labeled with GFP; however, we cannot currently confirm if they represent neurons and/or amphids.

By crossing *pezo-1::GFP* with a *tph-1*::DsRed marker–carrying strain, we were able to identify *pezo-1* expression in the pharyngeal neurosecretory, motor, and sensory (propioceptive/mechanosensory) neurons ($NSM_{L/R}$; Fig. 1 G). Importantly, these serotoninergic neurons have been proposed to sense food in the lumen of the pharynx through their proprioceptive-like endings and trigger feeding-related behaviors (i.e., increased pharyngeal pumping, decreased locomotion, and increased egg laying; Albertson and Thomson, 1976; Avery et al., 1993). In addition to the pharyngeal cells, we observed expression of *pezo-1* in the ventral nerve cord neurons, according to their morphology and location (Fig. 1 D), striated muscles (Fig. S1 C), coelomocytes (Fig. S1, D and E), spermatheca (Fig. S1, B and E), vulval muscles (Fig. S1 F), and various male neurons, including the ray neurons (Fig. S1 G). Our *pezo-1::GFP* expression patterns are consistent with those recently described in Hughes et al. (2021) (*Preprint*).

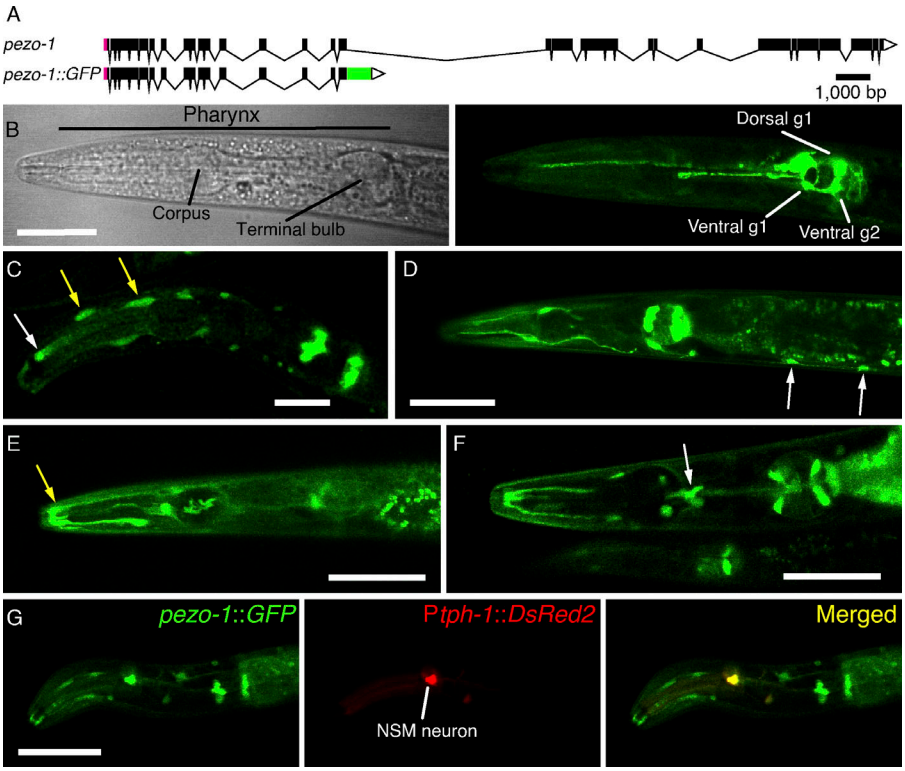

Figure 1. ***pezo-1* is strongly expressed in *C. elegans* pharynx. (A)** *pezo-1* gene diagram according to wormbase.org, release WS280 made with Exon-Intron Graphic Maker (wormweb.org). Magenta rectangles and white triangles denote the 5′ and 3′ UTRs, respectively; black rectangles denote exons; black lines denote introns; green rectangle denotes the GFP sequence inserted after exon 17. **(B)** Bright-field (left) and fluorescence (right) micrographs of the anterior end of a young adult *pezo-1::GFP* hermaphrodite highlighting pharynx structures and the GFP reporter expression in gland cells. Scale bar represents 50 µm. **(C)** Micrograph of the anterior end of a young adult *pezo-1::GFP* hermaphrodite expressing GFP in different cells. Arrows highlight pm3 muscle (white) and arcade cells (yellow), according to their morphology and location. Scale bar represents 20 µm. **(D and E)** Micrograph of the anterior end of a young adult *pezo-1::GFP* hermaphrodite expressing GFP in different cells. White and yellow arrows highlight ventral nerve cord neurons and posterior arcade syncytium, respectively, according to their morphology and location. Scale bar represents 50 µm. **(F)** Micrograph of the anterior end of a young adult *pezo-1::GFP* hermaphrodite expressing GFP in the pharyngeal sieve (white arrow), according to its morphology and location. Scale bar represents 100 µm. **(G)** Colocalization between *tph-1*::DsRed2 and *pezo-1::GFP* reporter in the NSM neuron. Scale bar represents 50 µm. Micrographs are representative of ≥20 independent preparations.

Importantly, the expression pattern reported by our *pezo-1* fosmid construct in NSM neurons matches what is reported in the *C. elegans* Neuronal Gene Expression Map & Network (CeNGEN; Taylor et al., 2021). The strong and varied *pezo-1* expression in the pharynx, along with the function of the cells expressing it, led us to investigate the potential contribution of PEZO-1 to pharyngeal function.

Serotonin stimulation reveals varying pharyngeal pump parameters

To analyze the contribution of *pezo-1* to pharyngeal pumping in *C. elegans*, we used the ScreenChip system (InVivo Biosystems), which can record electropharyngeograms (EPGs; Fig. 2 A; Raizen and Avery, 1994) by loading single, live worms into a microfluidic chip. Fig. 2, A and B, summarizes the pharynx anatomy, electrical properties measured during an EPG, and the neurons involved in pharyngeal function. For instance, the excitation event (E spike) precedes the pharyngeal contraction and is modulated by the MC pacemaker neuron (Fig. 2 B, top), whereas the repolarization event (R spike) leads to pharyngeal relaxation and correlates with the activity of the inhibitory M3 motor neurons (Fig. 2 B, middle). After three to four pumps, there is relaxation of the terminal bulb (isthmus peristalsis), which is modulated by the M4 motor neuron (Fig. 2 B, bottom; Avery and Horvitz, 1989). The main EPG events are regulated by the pharyngeal proprioceptive neuron, NSM. Importantly, the proprioceptive NSM neurons and the I3 interneuron express *pezo-1* according to our data (Fig. 1 G) and CeNGEN (Taylor et al., 2021), respectively.

Analysis of the EPG records allows for the determination of various pharyngeal pumping parameters, including frequency, duration, and the time interval that separates two pumping events (hereafter referred to as the interpump interval). We used serotonin to increase pharyngeal activity, since in the absence of food or serotonin, pumping events are infrequent. Serotonin mimics food stimulation by activating the $MC_{L/R}$ and $M3_{L/R}$ neurons (Niacaris and Avery, 2003). First, we established a serotonin dose–response profile of the WT (N2) strain pharyngeal pumping parameters (Fig. 2, C–G). Serotonin increases pharyngeal pumping frequency in a dose-dependent manner, with concentrations >5 mM increasing the likelihood of reaching 5 Hz (Fig. 2 C). We averaged the EPG recordings at each serotonin concentration and found a clear difference in pump duration between 0 and 5 mM. Concentrations ≥5 mM evoked similar pump durations (~100 ms; Fig. 2 D). Interestingly, analysis of the pump duration distribution profile under serotonin stimulation revealed that pharyngeal pump duration fits into two categories: fast (~80 ms) and slow (100–120 ms; Fig. 2 E, gray rectangles).

We observed that the fast and slow categories displayed an inverse relationship with respect to serotonin concentration (Fig. 2 E, arrows). Unlike pump duration, we observed only a single category for interpump interval, ~95–120 ms for serotonin concentrations of 5–20 mM (Fig. 2, F and G). Interestingly, we did not observe interpump intervals faster than 90 ms, regardless of the

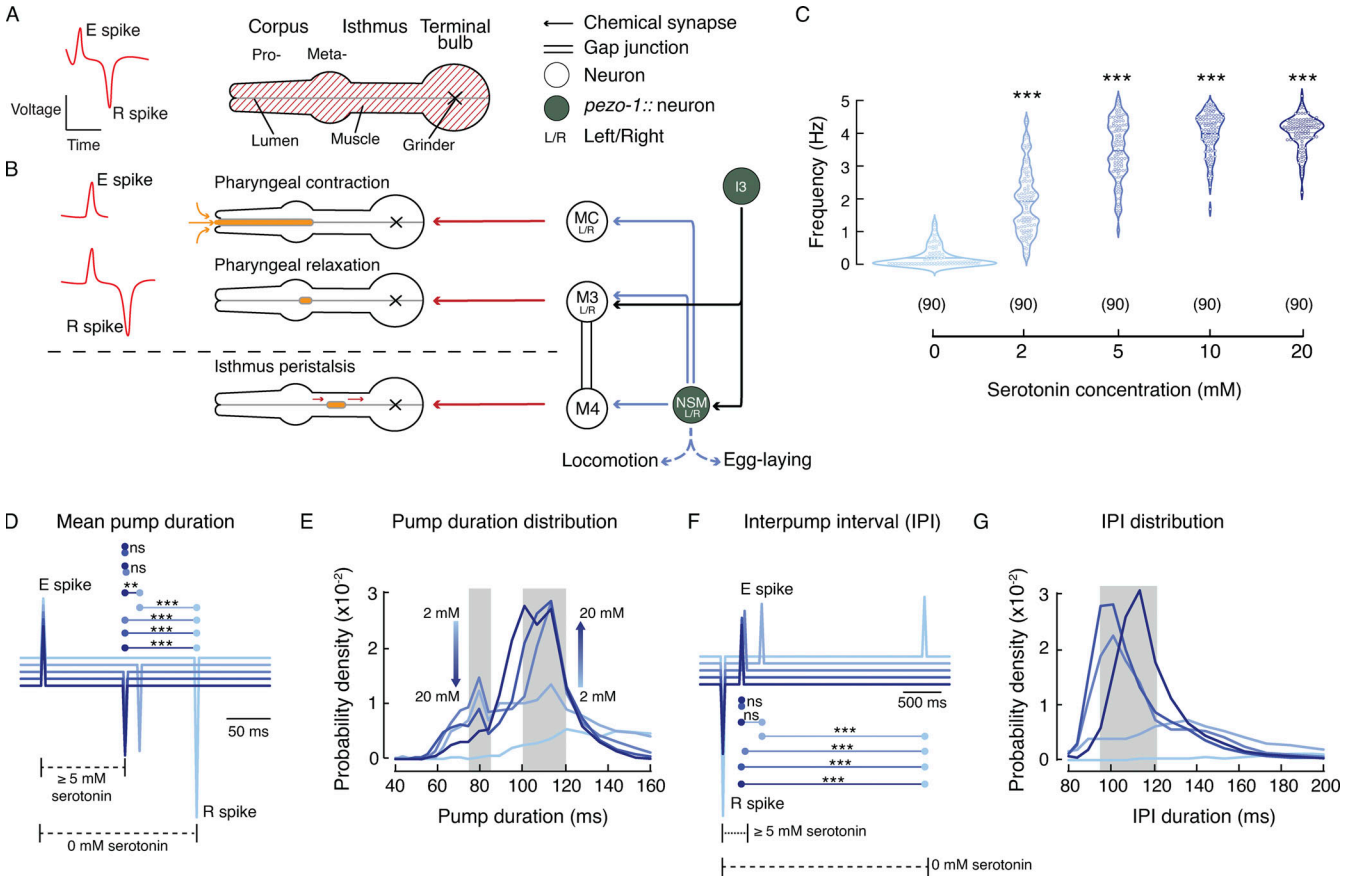

Figure 2. **Serotonin triggers pharyngeal pumping in a concentration-dependent manner in WT (N2) worms. (A)** Left: Illustration of an EPG recording depicting the contraction-relaxation of the corpus, referred to as pharyngeal pump. Right: Illustration representing the *C. elegans* pharyngeal muscle. **(B)** Representation of the main pharyngeal electrical coupling in *C. elegans*. Blue arrows represent serotoninergic transmission, red arrows represent neuromuscular junctions, double lines represent gap junctions, filled circles represent the neurons expressing *pezo-1* (NSM and I3 according to our data and CeNGEN [Taylor et al., 2021], respectively). **(C)** Pharyngeal pumping frequencies, depicted as violin plots with the means shown as horizontal bars, for WT (N2) at different serotonin concentrations. Kruskal–Wallis and Dunn's multiple comparisons tests (0 mM versus 2, 5, 10, and 20 mM). *n* is denoted above the x axis. **(D)** Ensemble averages of EPG traces for different serotonin concentrations showing pump durations (E to R spikes). One-way ANOVA and Tukey–Kramer multiple comparisons test. *n* = 90 worms per condition. **(E)** Serotonin concentration effect on pump duration. A kernel probability distribution was fit to the data. *n* = 90 worms per condition. **(F)** Ensemble averages of EPG traces for different serotonin concentrations showing interpump interval (R to E spikes). One-way ANOVA and Tukey–Kramer multiple comparisons test. *n* = 90 worms per condition. **(G)** Serotonin concentration effect on interpump interval. A kernel probability distribution was fitted to the data. *n* = 90 worms per condition. Asterisks indicate values that are significantly different (***, P < 0.001 and **, P < 0.01), and ns indicates not significantly different.

serotonin concentration. The interpump interval results support the idea that there is a minimum refractory period between two pumps. This set of analyses allowed us to establish a suitable model for evaluating the role of *pezo-1* function in vivo.

PEZO-1 modulates pump duration and interpump interval

To determine whether *pezo-1* has a functional role in pharyngeal pumping, we engineered LOF and GOF mutants. A putative LOF mutant was obtained by deleting 6,616 bp from the *pezo-1* locus (hereafter referred to as *pezo-1* KO; Fig. 3 A, top; and Fig. S2, A–C). This CRISPR-KO transgenesis deleted 638 amino acid residues from PEZO-1 that, according to the cryo-EM structure of the PIEZO1 mouse orthologue (Ge et al., 2015; Guo and MacKinnon, 2017; Saotome et al., 2018; Zhao et al., 2018), eliminates 12 transmembrane segments, 7 extra- and intracellular loops, and the beam helix that runs parallel to the plasma membrane (Fig. S2 D). Previous works demonstrated that the substitution of R2456H (located at the pore helix) in the human *Piezo1* gene orthologue increases cation permeability (GOF) and causes hemolytic anemia (Albuisson et al., 2013; Bae et al., 2013; Zarychanski et al., 2012). Moreover, a conservative substitution of Lys for Arg at position 2456 in the human PIEZO1 channel exhibits a pronounced slowed inactivation when compared with the WT or R2456H channels (Bae et al., 2013). Hence, we engineered a putative GOF mutant strain, obtained by substituting the conserved Arg 2373 with Lys (hereafter referred to as *pezo-1* R2373K or GOF; Fig. 3 A, bottom). Parenthetically, the R2373K numbering position is based on isoform G, one of the longest isoforms according to RNA sequencing (wormbase.org release WS280). We also included two mutants known to alter pharyngeal function, *eat-4(ad572)* and *avr-15(ad1051)*, in our analysis. EAT-4 is a glutamate-sodium symporter involved in postsynaptic glutamate reuptake. *eat-4(ad572)* affects the neurotransmission efficiency of all glutamatergic pharyngeal neurons

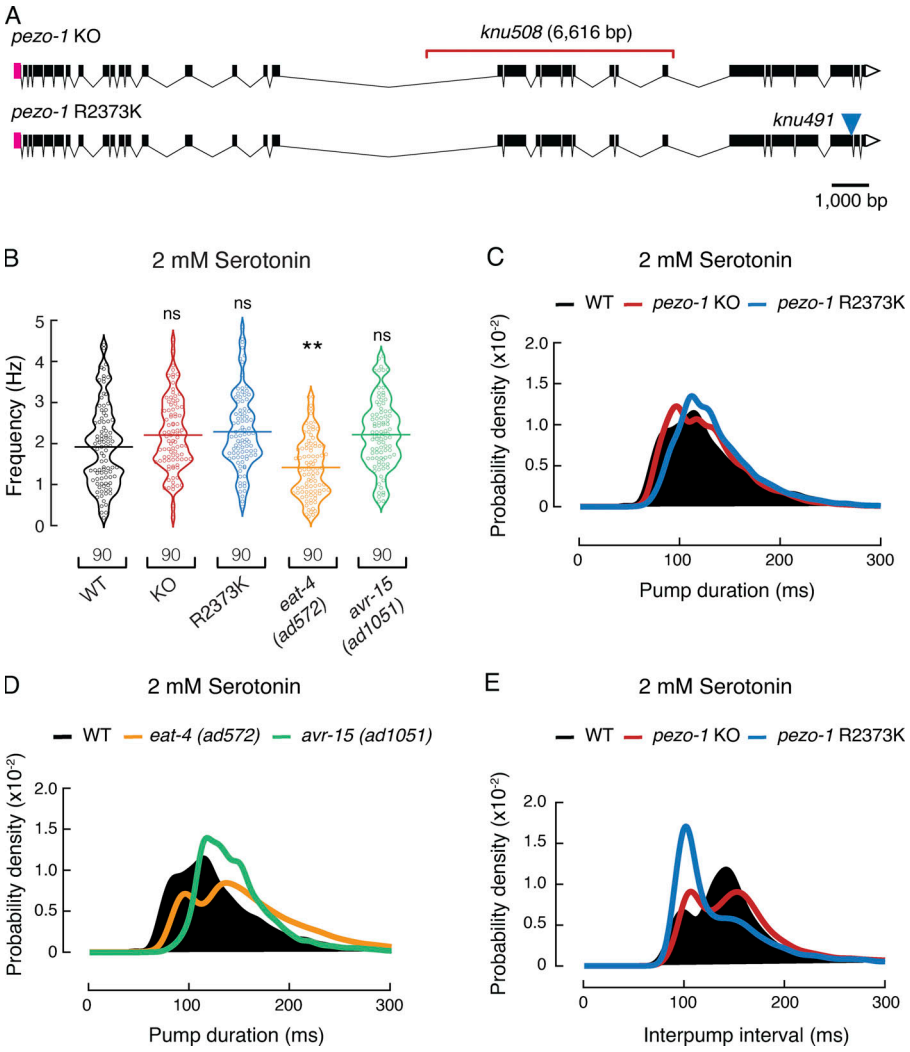

Figure 3. ***pezo-1* modulates pharyngeal pumping properties at 2 mM serotonin.** **(A)** *pezo-1* gene diagram according to wormbase.org release WS280 made with Exon-Intron Graphic Maker (wormweb.org). Magenta rectangles and white triangles denote the 5′ and 3′ UTRs, respectively; black rectangles denote exons; black lines denote introns; the red bracket denotes the *knu508* allele (a 6,616-bp deletion) of the *pezo-1* KO strain; and the blue triangle denotes the single point mutation (allele *knu491*) of the *pezo-1* R2373K strain. **(B)** Pharyngeal pumping frequencies depicted as violin plots with the means shown as horizontal bars for WT (N2), *pezo-1* KO, *pezo-1* R2373K, *eat-4 (ad572)*, and *avr-15 (ad1051)* strains. *n* is denoted above the x axis. Kruskal–Wallis and Dunn's multiple comparisons tests. Asterisks indicate values that are significantly different (**, $P < 0.01$), and ns indicates not significantly different. **(C)** Kernel density plot of WT, *pezo-1* KO, and *pezo-1* R2373K strain pump durations. *n* = 90 worms per condition. **(D)** Kernel density plot of WT, *eat-4 (ad572)*, and *avr-15 (ad1051)* strain pump durations. *n* = 90 worms per condition. **(E)** Kernel density plot of WT, *pezo-1* KO, and *pezo-1* R2373K strain interpump intervals. *n* = 90 worms per condition.

($I2_{L/R}$, I5, $M3_{L/R}$, M4, MI, and $NSM_{L/R}$; Lee et al., 1999). AVR-15 is a glutamate-gated chloride channel expressed in the pm4 and pm5 pharyngeal muscles (both synapsed by $M3_{L/R}$) and is involved in relaxation of the pharynx. Its mutant allele *ad1051* lengthens pump duration by delaying relaxation of the pharynx in a similar fashion to laser ablation of $M3_{L/R}$ neurons (Dent et al., 1997). With these strains, we sought to determine if altering PEZO-1 function would affect the worm's pharyngeal phenotype.

At a 2-mM concentration of exogenous serotonin (to elicit pharyngeal activity), both *pezo-1* KO and R2373K mutants displayed higher pumping frequencies than WT, albeit not statistically significantly (WT, 1.92 ± 0.11; KO, 2.21± 0.09; and GOF, 2.29 ± 0.1 Hz; mean ± SEM; Fig. 3 B), similar to *avr-15(ad1051)* (2.22 ± 0.09 Hz; mean ± SEM; Fig. 3 B). On the other hand, the *eat-4(ad572)* mutant displayed lower pumping frequency at this serotonin concentration. To further assess the altered pharyngeal function *pezo-1* mutants, we analyzed the pump duration distributions from the EPG records. *pezo-1* KO distribution is similar to the WT (Fig. 3 C, red versus black), whereas the R2373K mutant profile is reminiscent of *avr-15(ad1051)*, as both mutant strains displayed significantly narrower distributions around 100-ms pump events (Fig. 3, C and D, blue and green versus black), when compared with the WT (significance was determined by a *Z* test). Moreover, the R2373K mutant lacked fast pump events, 50–80 ms (Fig. 3 C), similar to the WT features observed at high serotonin concentrations (≥5 mM; Fig. 2 E) and the *eat-4(ad572)* and the *avr-15(ad1051)* mutants at a 2-mM serotonin concentration (Fig. 3 D). Analysis of the distribution of interpump intervals revealed that *pezo-1* KO and R2373K mutants, although different, both spend less time resting between pumps (95–120 ms) than the WT (≈140 ms; Fig. 3 E). This enhancement in function resembles the WT activity measured at 5–20-mM serotonin concentrations (Fig. 2, F and G) and could account for the slight increase in frequency shown in Fig. 3 B. The close resemblance between the pharyngeal pumping parameters of PEZO-1 GOF and the *avr-15(ad1051)* mutant suggests a potential link between PEZO-1 and pharyngeal relaxation.

PEZO-1 determines pharyngeal pumping in response to osmolarity

Mechanical stimuli come in many forms, including stretching, bending, and osmotic forces (Cox et al., 2019). To further understand the functional role of *pezo-1*, we evaluated pharyngeal

pumping parameters after challenging worm strains with varying osmolarities (in the absence of serotonin or food). The worm's pharynx draws in liquid and suspended bacteria from the environment and then expels the liquid but traps bacteria (Avery and You, 2012). We adjusted a standard laboratory solution used for worm experiments (M9 buffer, 320 mOsm) to varying osmolarities (150, 260, and 320 mOsm). Parenthetically, M9 buffer elicits acute withdrawal behavior in the absence of food, and another buffer (M13) with lower osmolarity (~280 mOsm) is commonly used to study molecules that elicit acute avoidance behavior (Hart et al, 2006; Jang and Bargmann, 2013; Caires et al, 2017, 2021; Geron et al, 2018). Because we measured the pharynx function in the absence of food for this set of experiments, we refer to the M9 buffer as a "high-osmolarity solution." Low-osmolarity solutions would be equivalent to swallowing liquid containing few solutes (150 mOsm), whereas high osmolarities would represent a "gulp" of liquid with a large amount of solutes (320 mOsm). Of note, higher osmolarities were associated with smaller mean pumping frequencies for WT worms (Fig. 4 A). Our results indicate that a larger number of solutes in solution corresponds to an increased retention time in the pharynx before moving to the intestine of the WT worms. Notably, at 260 mOsm, *pezo-1* mutants exhibited lower frequency than WT (albeit the KO was not statistically significant), and at 320 mOsm, both *pezo-1* KO and GOF mutants displayed a significantly higher pumping frequency than WT worms (Fig. 4 A). In contrast, we did not measure significant differences between WT worms and the *pezo-1* mutants at 150 mOsm. Akin to human Piezo2 KO or GOF mutations causing joint contractures (Chesler et al., 2016; Coste et al., 2013; McMillin et al., 2014), we demonstrated that lack of or enhanced PEZO-1 function modulated pharyngeal pumping frequencies similarly (at high osmolarities). Next, we further examined the EPG parameters at high osmolarity (320 mOsm). Analysis of the distribution of pump durations and length of the mean interpump intervals revealed that both *pezo-1* mutants had more frequent fast pumps (80–120 ms, Fig. 4 B), and the KO spent less time resting between pumps, compared with the WT (Fig. 4 C). Interestingly, high osmolarity (320 mOsm) revealed resemblances between PEZO-1 GOF and *avr-15(ad1051)* versus PEZO-1 KO and *eat-4(ad572)* pharyngeal pumping parameters (frequency and duration, Fig. 4, D and E). Altogether, our results suggest that PEZO-1 is required for fine-tuning pharyngeal function in response to osmolarity changes.

PEZO-1 function is involved in food sensation

To determine the impact that PEZO-1 function has on food intake, we recorded pharyngeal pumping of WT and *pezo-1* strains in response to varying food stimuli. It has been hypothesized that food quality and feeding preferences displayed by worms are linked to bacterial size (Shtonda and Avery, 2006). To this end, we measured worm pharyngeal pumping while feeding them with conventional food used in the laboratory for maintenance (*E. coli* strain OP50). We found that feeding WT worms *E. coli* elicited lower pumping frequencies than 2 mM serotonin (Fig. S3; *E. coli*, 1.36 ± 0.09; and serotonin, 1.92 ± 0.11 Hz; mean ± SEM), whereas *pezo-1* mutants displayed similar pumping frequencies with exogenous serotonin or *E. coli* (Fig. S3). Future experiments are needed to understand why exogenous serotonin stimulation and feeding result in varying *pezo-1* influence on pharyngeal function. Additionally, we varied the dimensions of OP50 using cephalexin, an antibiotic that prevents the separation of budding bacteria and generates long spaghetti-like filaments of bacterium, as observed under a microscope and elsewhere (Fig. S4 A; Hou et al., 2020; Martinac et al., 1987). Specifically, cephalexin yields bacteria whose contour length is 5–10 times longer and 1.5 times stiffer (i.e., Young's modulus and the bacterial spring constant) than untreated bacteria, as determined by fluorescence imaging and atomic force microscopy (Hou et al., 2020). Hence, feeding worms with these two physically different types of food could help to elucidate the physiological role of PEZO-1 in detecting food with varying mechanical properties (i.e., small and soft versus large and rigid food). A similar method was previously described using the antibiotic aztreonam and was shown to affect pharyngeal pumping (Ben Arous et al., 2009; Gruninger et al., 2008). WT and *pezo-1* mutants are able to ingest spaghetti-like bacteria and reached adulthood in 3 d, similar to worms fed with control bacteria (Fig. S4, B and C). Notably, feeding worms with control or spaghetti-like bacteria revealed distinctive pharyngeal traits between the *pezo-1* mutants and the WT worms (Fig. S4 D). When fed with control *E. coli*, both *pezo-1* mutants (KO and GOF) had higher mean frequencies, shorter mean pump durations, narrower pump duration distributions, and faster mean interpump intervals than the WT worms (Fig. 5, A–E). Conversely, feeding worms with spaghetti-like *E. coli* elicited opposing effects on the pharyngeal pumping parameters of the *pezo-1* mutants. For instance, feeding with spaghetti-like *E. coli* decreased *pezo-1* KO mean frequency, while the mean pump duration and distribution remained similar to WT worms (Fig. 5, A–C). Furthermore, this modified diet significantly increased the mean interpump interval of the KO in comparison to the GOF mutant (Fig. 5 D). Unlike the KO and WT strains, the R2373K *pezo-1* mutant displayed high-frequency, shorter pumps (mean and distributions; Fig. 5, A–C) and reduced mean interpump interval durations (mean and distributions; Fig. 5, D and E). Altogether, our results indicate that PEZO-1 regulates the pharynx response to the physical parameters of food, such as the length and stiffness of ingested bacteria.

pezo-1 encodes a mechanosensitive ion channel

The PEZO-1 protein sequence shares 60–70% similarity with mammalian PIEZO channel orthologues. However, whether PEZO-1 responds to mechanical stimuli has not yet been established. To address this major question, we cultured *C. elegans* cells from three different strains endogenously expressing *pezo-1* WT, KO, or the R2373K GOF mutation in the background of the VVR3 strain that expresses a nonfunctional *pezo-1::GFP* reporter (Fig. 1 A). *pezo-1* WT, KO, and GOF strains expressed similar levels of GFP (Fig. S5). Embryonic *pezo-1::GFP* cells were patch-clamped using the cell-attached configuration, with application of constant negative pressure (−70 mmHg) at different voltages (Fig. 6, A–C). The normalized steady-state current (I/I_{max})-versus-voltage relationship is characterized by a reversal potential of +9.06 mV (Fig. 6 D), indicating that PEZO-1 mediates a slight cation

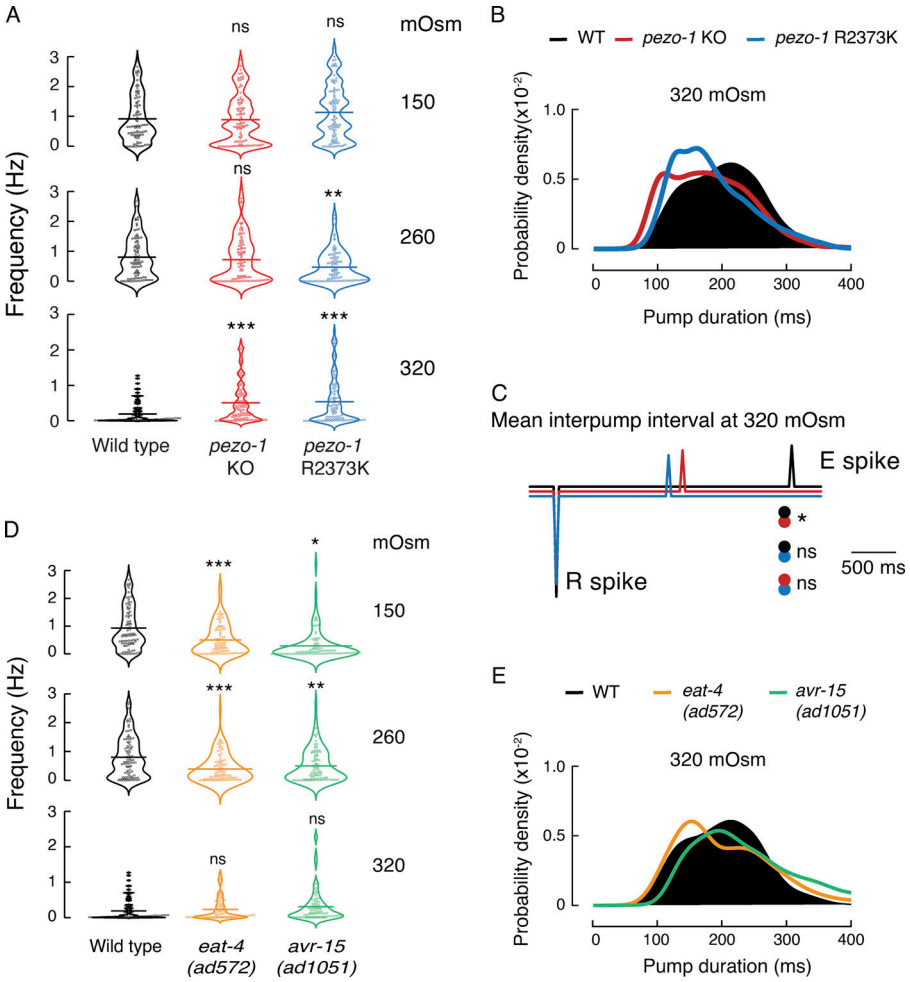

Figure 4. **Osmolarity changes modify pharyngeal pumping in WT and *pezo-1* strains, in the absence of serotonin. (A)** Pharyngeal pumping frequencies depicted as violin plots with the means shown as horizontal bars for WT (N2), *pezo-1* KO, and *pezo-1* R2373K strains at 150, 260, and 320 mOsm. *n* = 90 worms per condition. Kruskal–Wallis and Dunn's multiple comparisons tests. **(B)** Kernel density plot of WT, *pezo-1* KO, and *pezo-1* R2373K strain pump durations. *n* = 90 worms per condition at 320 mOsm. **(C)** Ensemble averages of EPG traces for WT (N2), *pezo-1* KO, and *pezo-1* R2373K strains showing interpump intervals (R to E spikes) at 320 mOsm (WT, 3,658.5 ± 2,747.0; KO, 2,369.3 ± 1,826.5; and GOF, 2,184.8 ± 2,013.2 ms; mean ± SEM). One-way ANOVA and Tukey–Kramer multiple comparisons test. *n* = 90 worms per condition. **(D)** Pharyngeal pumping frequencies depicted as violin plots with the means shown as horizontal bars for WT (N2), *eat-4 (ad572)*, and *avr-15 (ad1051)* strains at 150, 260, and 320 mOsm. *n* = 90 worms per condition. Kruskal–Wallis and Dunn's multiple comparisons tests. **(E)** Kernel density plot of WT, *eat-4 (ad572)*, and *avr-15 (ad1051)* strain pump durations at 320 mOsm. *n* = 90 worms per condition. Asterisks indicate values that are significantly different (***, P < 0.001; **, P < 0.01; and *, P < 0.05), and ns indicates not significantly different.

selective conductance, like the mouse and *Drosophila* orthologues (Coste, 2012). Importantly, most of the *pezo-1* WT cells displayed multiple-channel opening events upon mechanical stimulation. Nevertheless, from the few traces that carry pressure-dependent single-channel opening events, we were able to determine that PEZO-1 displays an outward slope conductance of 46.4 pS and an inward slope conductance of 34.8 pS (Figs. 6, E and F; and S6). These current magnitudes are similar to the conductance of human PIEZO1 (37.1 pS) reported by others (Gottlieb et al., 2012).

Mechanical stimulation of embryonic *pezo-1::GFP* cells expressing WT and GOF PEZO-1, but not the KO, yielded several channel openings upon increasing negative pressure (Fig. 7, A and C). As would be expected with increased activity, it was more difficult to identify single-channel opening events in the traces coming from the GOF, as compared with the WT (Figs. 7 B and S7). Cells expressing WT PEZO-1 displayed mechanodependent currents with a half-pressure activation ($P_{1/2}$) corresponding to −59.1 ± 4.3 mmHg (mean ± SEM; Fig. 7, A and D). Alternatively, PEZO-1 R2373K displayed mechanodependent currents with a significantly lower $P_{1/2}$ than the WT channel (−39.2 ± 2.2 mmHg; Fig. 7, A and D), indicating that the GOF mutant requires less mechanical stimulation to open. Since we could not reach saturating stimulus, these $P_{1/2}$ values might be inaccurate; hence, future experiments are needed to unequivocally determine the differences in sensitivity between the WT and GOF. Notably, the R2373K mutation introduced a latency for activation that was not detected in the WT (Fig. 7 A, blue traces; and Fig. 7 E). The decrease in mechanical threshold, along with the slowed activation, were previously reported for the equivalent human PIEZO1 R2456K mutation in mammalian cell lines (Albuisson et al., 2013; Bae et al., 2013; Romero et al., 2019; Zarychanski et al., 2012). Future experiments are needed to understand the origin of these differences in activation.

Unlike *pezo-1* WT, ∼50% of the mechanocurrents elicited from the *pezo-1* R2373K–expressing cells remained active after removal of the mechanical stimulus (Fig. 7 A, blue traces; Fig. 7 F; and Fig. S7). This slow deactivation is also reminiscent of the human PIEZO1 R2456K GOF phenotype previously characterized by Bae et al. (2013). Overall, our results suggest that PEZO-1 is a mechanosensitive ion channel and that a conserved mutation in the pore domain elicits activation and deactivation changes similar to those of its human counterpart.

One caveat of our PEZO-1 electrophysiological characterization in *C. elegans* cultured cells is that we cannot identify (at this point) which type of cells we are measuring from. We are only confident that those cells express *pezo-1* since they are labeled with the nonfunctional *pezo-1::GFP* reporter. These patch-clamp experiments were blind to genotype, yet we consistently found that *pezo-1::GFP*–labeled cells coming from KO worms had negligible or no currents under the same voltage and pressure

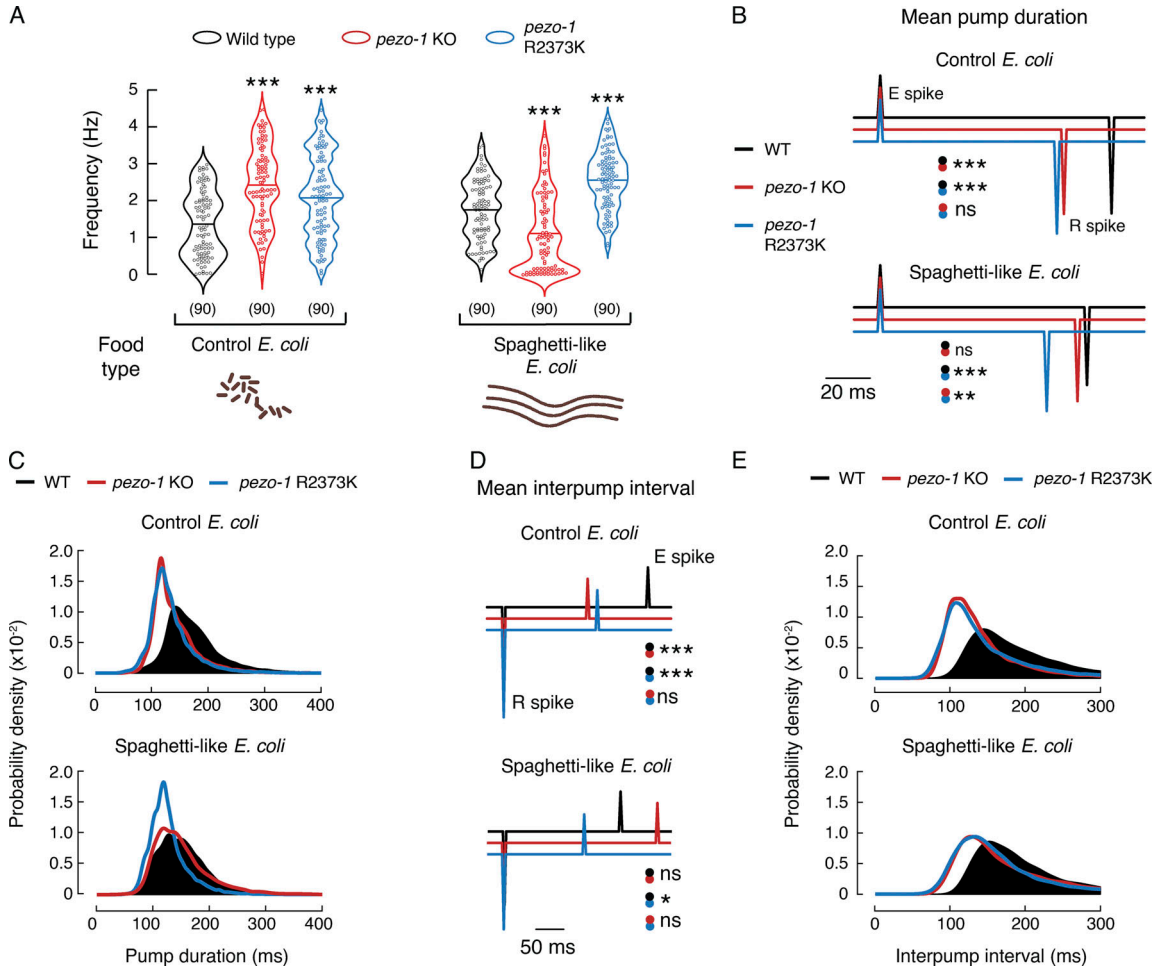

Figure 5. **PEZO-1 alters pharyngeal pumping when exposed to control or spaghetti-like bacteria. (A)** Pharyngeal pumping frequencies depicted as violin plots with the means shown as horizontal bars, for WT (N2), *pezo-1* KO, and *pezo-1* R2373K strains when fed with control or cephalexin-treated *E. coli* (spaghetti-like bacteria). Bacteria cartoon depictions were created with BioRender.com. *n* is denoted above the x axis. Kruskal–Wallis and Dunn's multiple comparisons tests. **(B)** Ensemble averages of EPG traces for WT (N2), *pezo-1* KO, and *pezo-1* R2373K strains showing pump durations (E to R spikes), when fed with control or cephalexin-treated bacteria (spaghetti-like *E. coli*; control: WT, 190.1 ± 47.7; KO, 142.5 ± 25.6; and GOF, 135.9 ± 23.3 ms; spaghetti: WT, 170.4 ± 40.4; KO, 161.8 ± 36.9; and GOF, 130.6 ± 21.5 ms; mean ± SEM). One-way ANOVA and Tukey–Kramer multiple comparisons test. *n* = 90 worms per condition. **(C)** Kernel density plot of WT, *pezo-1* KO, and *pezo-1* R2373K strains pump durations when fed with control or cephalexin-treated bacteria. *n* = 90 worms per condition. **(D)** Ensemble averages of EPG traces for WT (N2), *pezo-1* KO, and *pezo-1* R2373K strains showing interpump interval (R to E spikes), when fed with control or cephalexin-treated bacteria (control: WT, 853.3 ± 523.0; KO, 433.0 ± 178.2; and GOF, 496.3 ± 232.1 ms; spaghetti: WT, 565.0 ± 216.8; KO, 848.2 ± 613.8; and GOF, 391.6 ± 108.8 ms; mean ± SEM). One-way ANOVA and Tukey–Kramer multiple comparisons test. *n* = 90 worms per condition. **(E)** Kernel density plot of WT, *pezo-1* KO, and *pezo-1* R2373K strain interpump interval when fed with control or cephalexin-treated bacteria. *n* = 90 worms per condition. Asterisks indicate values that are significantly different (***, P < 0.001; **, P < 0.01; and *, P < 0.05), and ns indicates not significantly different.

regimes used for *pezo-1* WT and GOF cell cultures (Fig. 7 C). Hence, to further validate that the *pezo-1* gene encodes for a mechanosensitive ion channel, we heterologously expressed one of the longest isoforms of *pezo-1* (isoform G; wormbase.org release WS280) in Sf9 cells and measured its function in the whole-cell patch-clamp configuration while stimulating with a piezo-electrically driven glass probe (Fig. 8 A). Similar to mammalian PIEZO channels, PEZO-1 mediates indentation-activated currents (Fig. 8 B). Uninfected Sf9 cells do not display mechanosensitive channel currents (Figs. 8 B and S8). Importantly PEZO-1 displayed the properties described for mammalian PIEZOs in other cell types (Coste et al., 2010; Wu et al., 2017b), including voltage-dependent inactivation (Fig. 8, C–F) and nonselective cation currents, as determined by the reversal potential (−1.15 mV; Fig. 8 G). Our results demonstrate that expressing *pezo-1* in a naive system was sufficient to confer mechanosensitivity to Sf9 cells.

We also evaluated the PEZO-1 R2373K mutation in Sf9 cells and found that, like the human equivalent (Bae et al., 2013), the GOF elicits larger mechanically evoked currents that inactivate more slowly than the WT channel (Fig. 8, B–F; and Fig. S8). WT and GOF PEZO-1 channels are characterized by similar reversal potentials and unitary conductance, as determined by whole-cell and inside-out patches, respectively (Fig. 8, G and H; and Fig. S9). As previously reported with human PIEZO1 (Bae et al., 2013), we found that PEZO-1 (WT and GOF) features unique characteristics when activated with two different types of mechanical stimuli (negative pressure or displacement). For instance, with negative

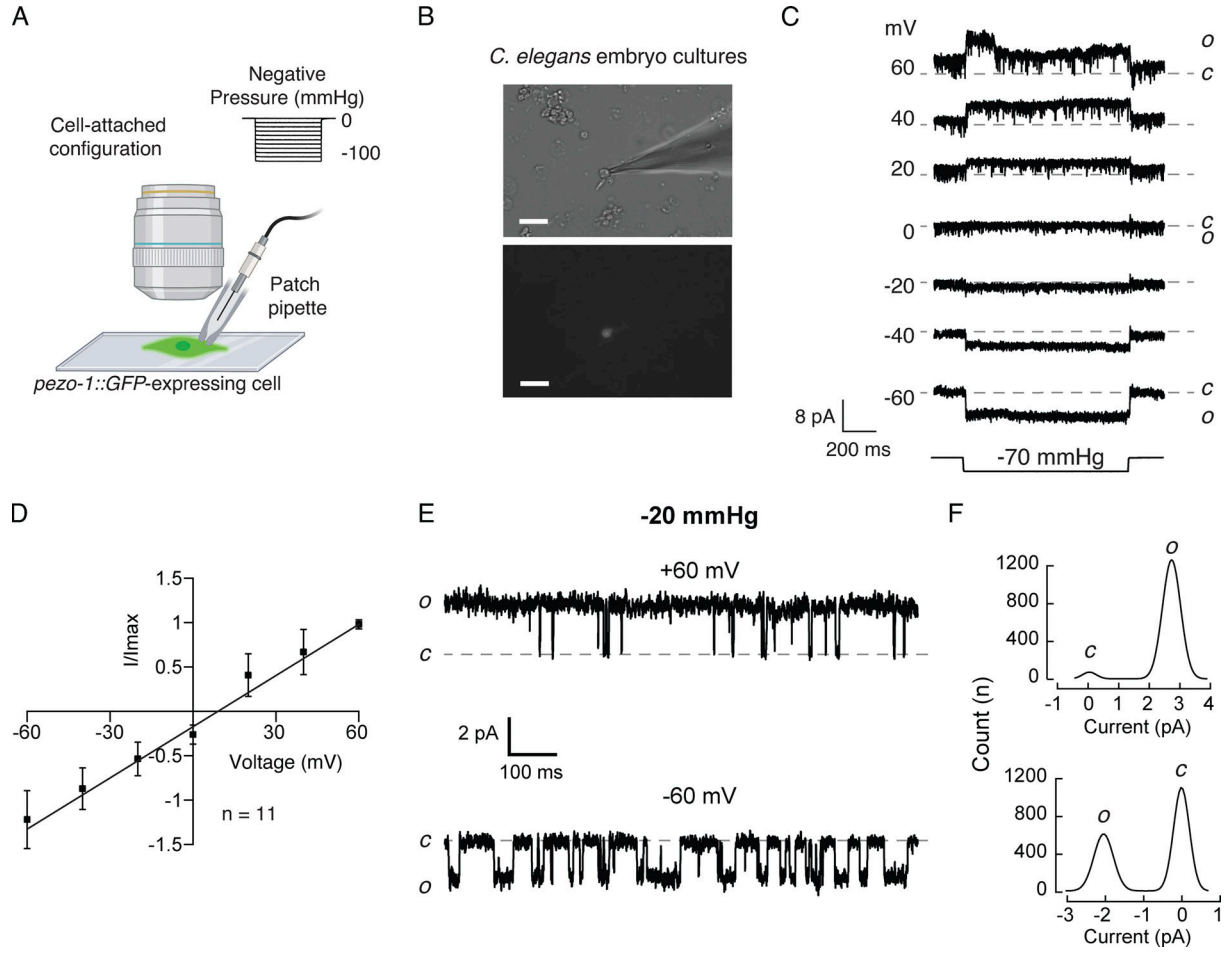

Figure 6. **Cells expressing PEZO-1 display mechanosensitive channel currents. (A)** Schematic representation of the mechanical stimulation protocol applied to *pezo-1::GFP*–expressing cells recorded in the cell-attached configuration. Created with BioRender.com. **(B)** Representative micrographs (from ≥10 independent preparations) of a *C. elegans* primary embryonic culture from *pezo-1::GFP*–expressing strains. Bright-field (top) and fluorescence (bottom) micrographs of a *pezo-1::GFP*–expressing cell when patch-clamped in the on-cell configuration. Scale bar represents 20 µm. **(C)** Representative cell-attached patch-clamp recordings of mechanically activated currents of WT cells expressing *pezo-1::GFP*. Channel openings were elicited by application of a −70-mmHg-square pulse (bottom) at constant voltages ranging from −60 to +60 mV. Dashed gray line represents background currents. Closed and open states are labeled *c* and *o*, respectively. **(D)** Normalized current–voltage relationship recorded at constant pressure in the cell-attached configuration. The reversal potential is 9.06 mV. Each square represents the mean ± SD. **(E)** Representative single-channel trace recordings of WT cells expressing *pezo-1::GFP* in the cell-attached configuration. Channel openings were elicited by −20 mmHg of negative pressure at constant voltages (+60 or −60 mV). Closed and open states are labeled *c* and *o*, respectively. **(F)** All-point amplitude histograms of pressure-evoked single-channel currents from recordings shown in E.

pressure, WT and mutant channels displayed steady-state currents, but only the GOF mutant exhibited a pronounced latency for activation and slowed deactivation. With displacement stimulation, it is possible to determine that PEZO-1 GOF inactivates more slowly than the WT. Overall, our results indicate that PIEZO orthologues are functionally conserved.

Discussion

In 2010, Coste and collaborators reported that the *C. elegans* genome contained a single *Piezo* gene, *pezo-1* (Coste et al., 2010). However, the functional role of *pezo-1* remained elusive, even a decade after its discovery. Here, we showed that PEZO-1 is a mechanosensitive channel with a novel functional role in the worm pharynx by combining fluorescent reporters, genome editing, EPG recordings, behavior, and patch-clamp measurements. We found that *pezo-1* is highly expressed in gland cells and the proprioceptive-like NSM neuron, among many other tissues. In addition to its expression, several lines of evidence suggested that PEZO-1 modulated several discrete but reliable features of pharyngeal function. Lack or augmentation of PEZO-1 function decreased interpump intervals when worms were challenged with 2 mM serotonin, while it also increased pumping frequency in high-osmolarity conditions or feeding with control bacteria. In the absence of functional PEZO-1, worms had reduced pharyngeal function (i.e., low frequency and long pump intervals) when fed with spaghetti-like bacteria. Finally, we demonstrated that the *pezo*-1 gene (WT or GOF) encodes a mechanosensitive ion channel by measuring its native function in *C. elegans* cells or with heterologous expression in insect cells. Altogether, our results established that PEZO-1 is important for pharyngeal function, regulation, and food sensation.

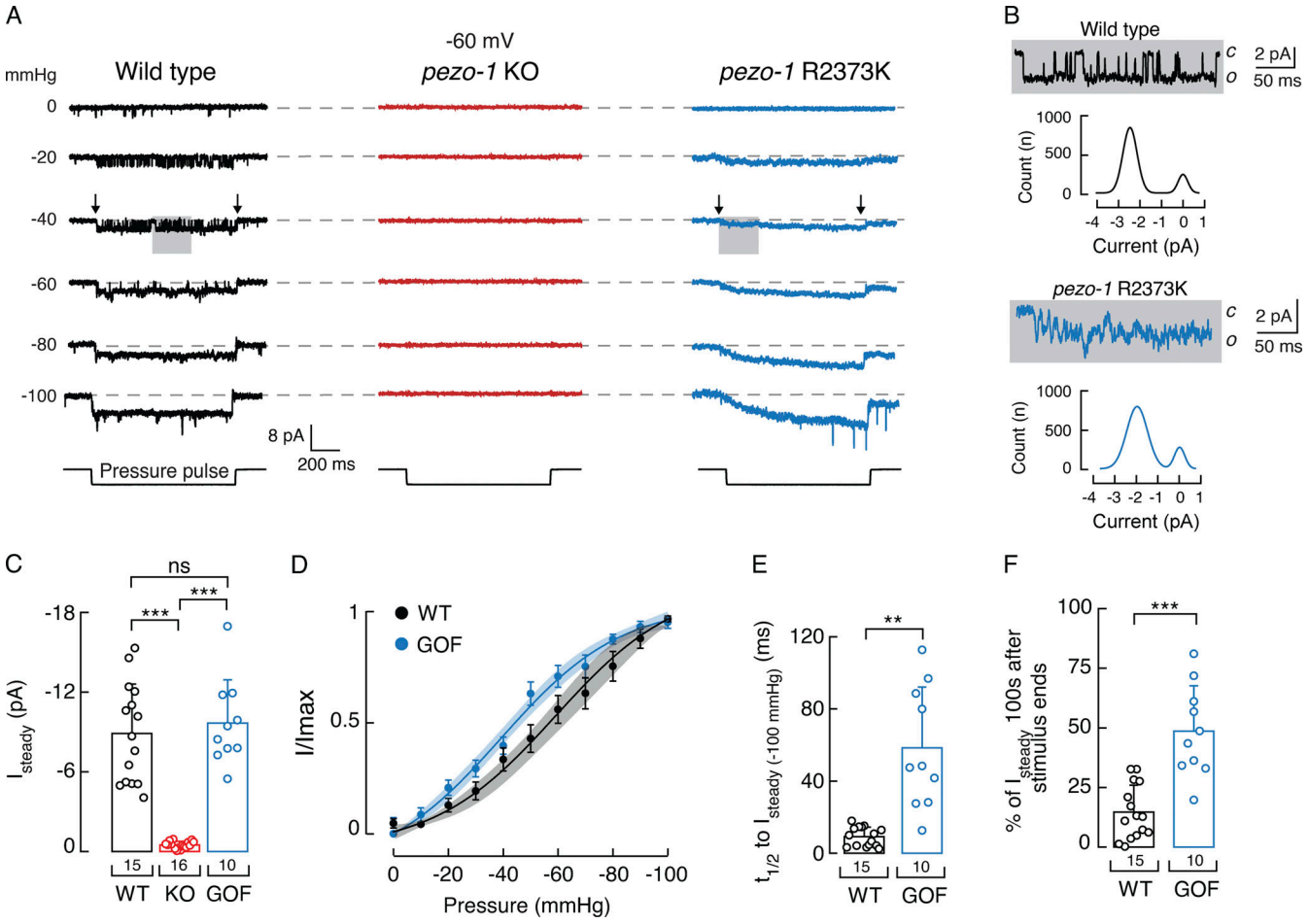

Figure 7. ***pezo-1* GOF mutant decreases the mechanical threshold and slows down deactivation. (A)** Representative cell-attached patch-clamp recordings of mechanically activated currents from WT, *pezo*-1 KO, and *pezo-1* R2373K cells expressing *pezo-1::GFP*. Channel openings (downward) were elicited by negative pressure (left) square pulses (bottom) at a constant voltage of −60 mV. Dashed gray line represents background currents; gray rectangles highlight records magnified in B; black arrows mark the recording sections (see filtered records on Fig. S7) used to generate the all-point amplitude histograms shown in B. **(B)** Gray rectangles show higher magnifications of indicated pressure-evoked responses shown in A. Traces are accompanied by all-point amplitude histograms generated from the corresponding records highlighted by arrows in A. **(C)** Bar graph displaying steady-state currents elicited by −100 mmHg of negative pressure of WT, *pezo*-1 KO, and *pezo-1* R2373K cells expressing *pezo-1::GFP*. Bars are mean ± SD. *n* is denoted above the x axis. Kruskal–Wallis and Dunn's multiple comparisons tests. **(D)** Pressure-response profiles for *pezo-1* WT and R2373K currents. Normalized currents (I/I_{max}) elicited by negative pressure of mechanically activated currents of WT and *pezo-1* R2373K cells expressing *pezo-1::GFP*. A Boltzmann function, Eq. 1, was fitted to the data. The shadows encompassing the curves indicate the 95% confidence bands for the fit. Circles are mean ± SD. *n* = 15 for WT and *n* = 10 for *pezo-1* R2373K. **(E)** Bar graph displaying the time it takes to reach half of the steady-state currents, elicited by −100 mmHg of pressure, of WT and *pezo-1* R2373K cells expressing *pezo-1::GFP*. Bars are all mean ± SD. *n* is denoted above the x axis. Unpaired *t* test with Welch's correction. **(F)** Bar graph displaying the percentage of steady-state currents remaining 100 ms after the removal of the mechanical stimulus, from WT and *pezo-1* R2373K cells expressing *pezo-1::GFP*. Bars are mean ± SD. *n* is denoted above the x axis. Unpaired *t* test. Asterisks (***, P < 0.001 and **, P < 0.01) indicate values that are significantly different, and ns indicates not significantly different..

C. elegans feeding relies on the ability of the pharynx to contract and relax. The pharynx is a tube of electrically coupled muscle cells that pump continuously throughout the worm's life (Mango, 2007). Several ion channels have been identified to be crucial for the pharyngeal muscle action potential, including acetylcholine receptors, T- and L-type Ca^{2+} channels, glycine receptors, and K^+ channels (Avery and You, 2012). Although the pharyngeal muscle is capable of pumping (albeit at low frequencies) without nervous system input, higher pumping frequencies are controlled by pharyngeal motor neurons, namely $MC_{L/R}$ and $M3_{L/R}$ (Avery and You, 2012). Nevertheless, the role of the nervous system in the control of rhythmic pharyngeal pumping is not completely understood. It is known, however, that the pharynx responds to a variety of neuromodulators (Avery and Horvitz, 1989). We found that *pezo-1* is expressed in proprioceptive/mechanosensory $NSM_{L/R}$ neurons (which are important for the pharyngeal nervous system). Moreover, Taylor et al. (2021) reported expression of *pezo-1* in the pharyngeal I3 interneuron. Unlike $NSM_{L/R}$ and $M3_{L/R}$, the function of I3 has not been established (Avery, 1993; Avery and Thomas, 1997). Our results suggest that PEZO-1 is not essential for pharyngeal muscles, but instead fine-tunes the role of the nervous system in controlling pharynx function. This is reminiscent of the novel role of mammalian PIEZO1 and PIEZO2 in mediating

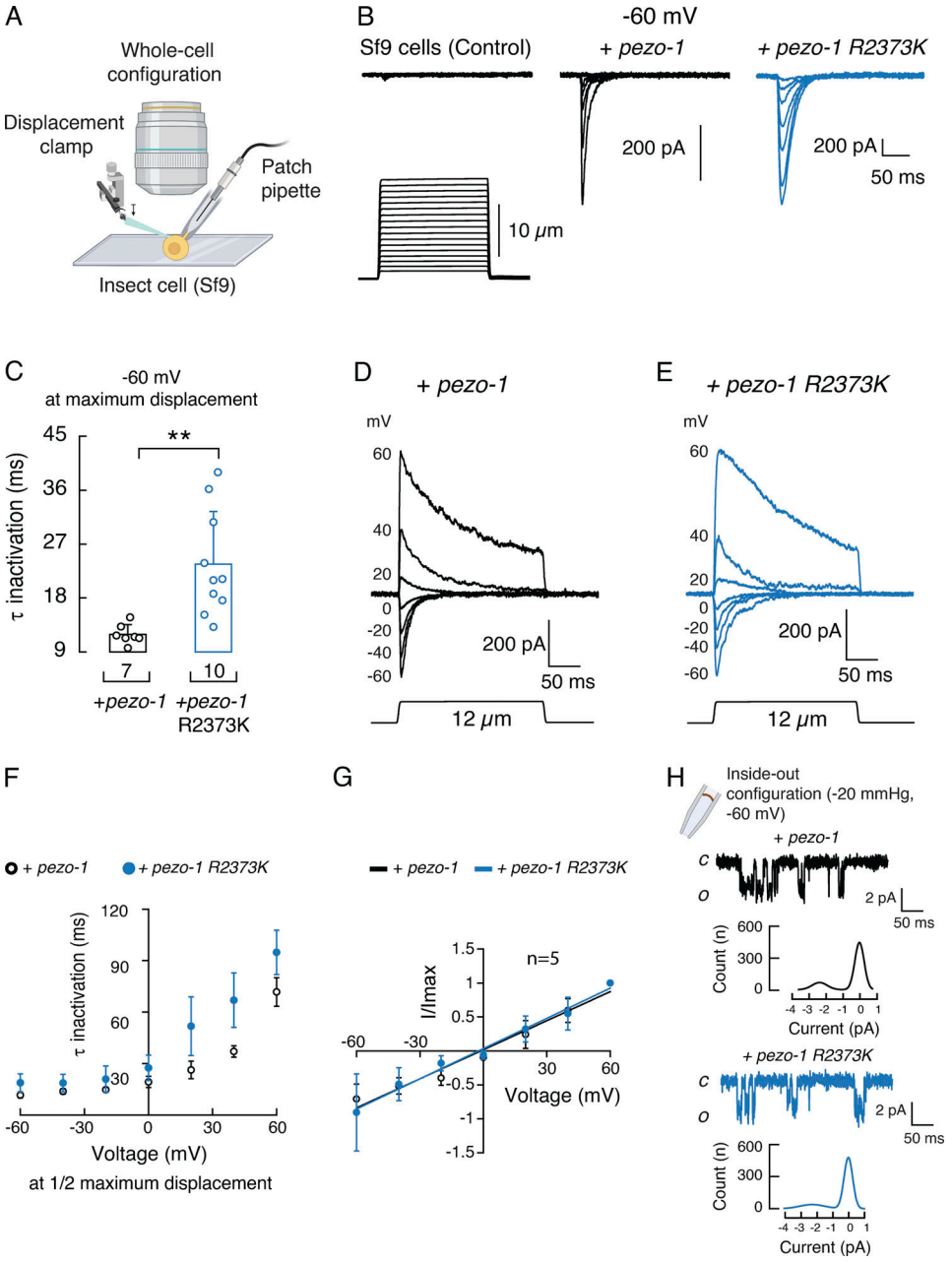

Figure 8. **Sf9 cells infected with *pezo-1* WT- or *R2373K*-containing baculovirus display mechanosensitive currents. (A)** Schematic representation of the mechanical stimulation protocol applied to Sf9 cells infected with baculovirus containing *pezo-1* (WT or R2373K constructs) recorded in the whole-cell configuration. Created with BioRender.com. **(B)** Representative whole-cell patch-clamp recordings (at −60 mV) of currents elicited by mechanical stimulation of Sf9 cells, uninfected (control), or expressing *pezo-1* WT or R2373K. **(C)** Time constants of inactivation elicited by maximum displacement (−60 mV) of Sf9 cells expressing *pezo-1* WT or R2373K. Bars are mean ± SD. Two-tailed unpaired *t* test with Welch correction. **(D)** Representative whole-cell patch-clamp recordings (top) at constant voltages (ranging from −60 to +60 mV) of currents elicited by mechanical stimulation (bottom) of Sf9 cells expressing *pezo-1* WT. **(E)** Representative whole-cell patch-clamp recordings (top) at constant voltages (ranging from −60 to +60 mV) of currents elicited by mechanical stimulation (bottom) of Sf9 cells expressing *pezo-1* R2373K. **(F)** Time constants of inactivation elicited by one-half maximum displacement at constant voltages ranging from −60 to +60 mV, of Sf9 cells expressing *pezo-1* WT (n = 5) or R2373K (n = 5). Each circle represents the mean ± SD. **(G)** Normalized current–voltage relationship, recorded in the whole-cell configuration at a constant displacement of 12 µm. The reversal potential is −1.15 and −2.23 mV for *pezo-1* WT and R2373K, respectively. Each circle represents the mean ± SD. **(H)** Representative single-channel trace recordings and all-point amplitude histograms of pressure-evoked currents from Sf9 cells expressing *pezo-1* WT or R2373K, recorded in the inside-out configuration. Channel openings were elicited by −20 mmHg of negative pressure at −60 mV. Closed and open states are labeled *c* and *o*, respectively. **, P < 0.01.

neuronal sensing of blood pressure and the baroreceptor reflex (Zeng et al., 2018).

$NSM_{L/R}$ and $M3_{L/R}$ ($NSM_{L/R}$ are *pezo-1*–expressing neurons), have been postulated to sense bacteria in the pharynx lumen, via their proprioceptive endings, and secrete serotonin in response to this mechanical stimulus (Avery, 1993; Avery and Thomas, 1997). Laser ablation of $NSM_{L/R}$ in *unc-29* mutants leads to subtle changes in pharyngeal pumping rate; however, this was done while simultaneously ablating other pharyngeal motor neurons (M1, $M2_{L/R}$, $M3_{L/R}$, M5, and MI; Avery, 1993). This approach could exert antagonistic effects on pumping rate, yielding a steady pharyngeal activity. Using the ScreenChip system allowed us to reveal the potential roles of extrapharyngeal neurons expressing *pezo-1* ($NSM_{L/R}$). Our results determined that proper function of PEZO-1 lengthened interpump intervals with 2 mM serotonin, in the absence of food. They further demonstrated that PEZO-1 modulated the feeding behavior of worms confronted with food of various mechanical properties (control and spaghetti-like bacteria). This led us to hypothesize that PEZO-1 is involved in food sensation and modulates pharyngeal pumping rate. Hence, like the mammalian orthologue PIEZO2, PEZO-1 is expressed in proprioceptive endings and is involved in stretch reflexes (Chesler et al., 2016; Woo et al., 2015). Nevertheless, it remains to be determined if mammalian PIEZO channels play a role in food sensation and/or the swallowing reflex.

Humans sense various organoleptic food qualities, such as visual aspects (color and shape), odorants through smell, and texture and flavor through tasting. In nematodes, there is a lack of understanding of what is sensed as food. Worms are able to filter particles from fluid in a size-dependent manner (Fang-Yen et al., 2009; Kiyama et al., 2012), and feeding is facilitated by attractive odors or suppressed by repellents (e.g., diacetyl, isoamyl alcohol, quinine; Gruninger et al., 2008; Li et al., 2012). Others have demonstrated that worms prefer to feed from active (i.e., bacteria reproducing rapidly and emitting high levels of CO_2) rather than inactive bacteria (Yu et al., 2015). We determined that *pezo-1* KO worms "choke" when presented with long and stiff spaghetti-like bacteria, whereas WT and GOF strains increase pharyngeal pumping when ingesting this elongated and rigid food. Therefore, we propose that the pharynx itself might be a sensory organ, as worms modify their pumping parameters when they sense solutions of different osmolarities or food with different textures and/or consistencies. We further hypothesize that worms can perceive changes in texture and adjust their pumping frequency through a mechanism requiring PEZO-1. Since *pezo-1* is not essential for *C. elegans* when cultured in standard laboratory conditions (e.g., monoaxenically on *E. coli* OP50), we wonder if in its natural biotic environment this mechanosensitive ion channel plays a crucial role, as it does in humans and *Drosophila*. Given that worms grow in microbe-rich and heterogeneous environments (feeding from prokaryotes of the genera *Acetobacter*, *Gluconobacter*, and *Enterobacter*, for example; Schulenburg and Félix, 2017), they might encounter bacteria of different dimensions and stiffness that would make *pezo-1* function more relevant to the worm's ability to discriminate the food on which it grows best.

Why do *pezo-1* LOF and GOF mutations cause similar behavioral phenotypes? Our data show that both *pezo-1* mutants (KO and GOF) increase the pumping frequency of the pharynx in different settings: serotonin exposure (albeit not statistically significantly), high osmolarity, and ingestion of control bacteria. While it may seem counterintuitive at first, there are some scenarios in which too little or too much mechanosensation can be detrimental for animal behavior. In humans, *PIEZO2* LOF (premature stop codon) and GOF (missense mutation I802F) alleles cause joint contractures, skeletal abnormalities, and alterations in muscle tone (Chesler et al., 2016; Coste et al., 2013; Yamaguchi et al., 2019). Only when feeding worms with spaghetti-like bacteria were we able to uncover differences in the pharyngeal parameters between the LOF and GOF mutants. Hence, we hypothesize that lacking the function of PEZO-1 significantly slows pharyngeal function when passing the lengthy and rigid bacteria from the pharynx to the gut.

Several requirements must be met for a channel to be considered mechanically gated (Arnadóttir and Chalfie, 2010). Accordingly, we found that *pezo-1* is expressed in the proprioceptive NSM neuron; knocking out *pezo-1* inhibits worm pharyngeal function when fed with elongated and stiff bacteria; engineering a single point mutation in the putative pore domain (R2373K) elicited similar inactivation, activation, and deactivation delays that are reminiscent of the gating behavior reported for the human PIEZO1 R2456K (Bae et al., 2013); and expression of *pezo-1* (WT and GOF) confers mechanosensitivity to, otherwise naive, Sf9 cells. We propose that PEZO-1 is a mechanosensitive ion channel given that the time it takes to reach half of the steady-state currents ranges between 3.5 and 15 ms upon application of negative pressure. These are faster than activation times reported for the *Drosophila* phototransduction cascade, one of the most rapid second messenger cascades (Hardie, 2001). These combined efforts highlight the versatile functions of the PIEZO mechanosensitive channel family, as well as the strength of the *C. elegans* model organism to reveal physiological functions.

Our findings revealing PEZO-1 as a mechanosensitive ion channel that modulates pharyngeal function raise several important questions. How does *pezo-1* modulate pumping behavior electrical activity? Does *pezo-1* equally enhance or inhibit the function of the pharyngeal hypodermal, gland, and muscle cells, as well as neurons, expressing this channel? Could *pezo-1* phenotypes be exacerbated if the gene function is nulled in a cell-specific manner? Does the slow deactivation and/or inactivation of the GOF mutant, determined at the patch-clamp level, account for the enhancement in pharyngeal function when worms are fed with bacteria? Does PEZO-1 require auxiliary subunits and/or the cytoskeleton for gating? Regardless of the answers, the plethora of physiologic roles that this eukaryotic family of mechanosensitive ion channels play is outstanding. More experimental insight will be needed to fully grasp the full implications of *pezo-1* in the physiology of *C. elegans*.

Data availability

Data supporting the findings of this paper are available from the corresponding author upon reasonable request. The source data underlying figures and supplementary figures are provided as a

Source Data file, doi: https://doi.org/10.6084/m9.figshare.16992058.v3.

Acknowledgments

Jeanne M. Nerbonne served as editor.

We thank Dr. Julio F. Cordero-Morales, Dr. Andrés G. Vidal-Gadea, and Dr. Christopher E. Hopkins for critically reading the manuscript, as well as Dr. Rebeca Caires and graduate students Olufunke Falayi and Soumi Mazumdar for technical assistance. LX960 was provided by Dr. Kevin Collins (University of Miami).

C. elegans (N2, DA572, and DA1051) and *E. coli* strains (OP50 and NA22) were obtained from the *Caenorhabditis* Genetics Center, which is funded by the National Institutes of Health Office of Research Infrastructure Programs (P40 OD010440). This work was supported by the American Heart Association (16SDG26700010 to V. Vásquez) and the National Institutes of Health (R01GM133845 to V. Vásquez), as well as the Neuroscience Institute, University of Tennessee Health Science Center (Research Associate Matching Salary Support to J. Lee).

The authors declare no competing financial interests.

Author contributions: Conceptualization, V. Vásquez; Formal Analysis, V. Vásquez, J.R.M. Millet, and L.O. Romero; Funding Acquisition, V. Vásquez; Investigation, J.R.M. Millet, L.O. Romero, J. Lee, and B. Bell; Methodology, V. Vásquez and J.R.M. Millet; Project Administration, V. Vásquez; Supervision, V. Vásquez; Writing-original draft, V. Vásquez and J.R.M. Millet; Writing-review and editing, V. Vásquez.

Submitted: 11 May 2021
Revised: 28 October 2021
Accepted: 12 November 2021

References

Albertson, D.G., and J.N. Thomson. 1976. The pharynx of Caenorhabditis elegans. *Philos. Trans. R. Soc. Lond. B Biol. Sci.* 275:299–325. https://doi.org/10.1098/rstb.1976.0085

Albuisson, J., S.E. Murthy, M. Bandell, B. Coste, H. Louis-Dit-Picard, J. Mathur, M. Fénéant-Thibault, G. Tertian, J.P. de Jaureguiberry, P.Y. Syfuss, et al. 2013. Dehydrated hereditary stomatocytosis linked to gain-of-function mutations in mechanically activated PIEZO1 ion channels. *Nat. Commun.* 4:1884. https://doi.org/10.1038/ncomms2899

Alper, S.L. 2017. Genetic Diseases of PIEZO1 and PIEZO2 Dysfunction. *Curr. Top. Membr.* 79:97–134. https://doi.org/10.1016/bs.ctm.2017.01.001

Altun, Z.F., and D.H. Hall. 2009. Epithelial system, interfacial cells. In WormAtlas. doi:. https://doi.org/10.3908/wormatlas.1.15

Arnadóttir, J., and M. Chalfie. 2010. Eukaryotic mechanosensitive channels. *Annu. Rev. Biophys.* 39:111–137. https://doi.org/10.1146/annurev.biophys.37.032807.125836

Avery, L. 1993. Motor neuron M3 controls pharyngeal muscle relaxation timing in Caenorhabditis elegans. *J. Exp. Biol.* 175:283–297. https://doi.org/10.1242/jeb.175.1.283

Avery, L., and H.R. Horvitz. 1989. Pharyngeal pumping continues after laser killing of the pharyngeal nervous system of C. elegans. *Neuron.* 3:473–485. https://doi.org/10.1016/0896-6273(89)90206-7

Avery, L., and J.H. Thomas. 1997. Feeding and Defecation. *In:* D.L. Riddle, T. Blumenthal, B.J. Meyer, and J.R. Priess. (eds.) C. elegans II. Cold Spring Harbor Laboratory Press, Cold Spring Harbor, NY.

Avery, L., and Y.J. You. 2012. C. elegans feeding. *WormBook.*:1–23.

Avery, L., C.I. Bargmann, and H.R. Horvitz. 1993. The Caenorhabditis elegans unc-31 gene affects multiple nervous system-controlled functions. *Genetics.* 134:455–464. https://doi.org/10.1093/genetics/134.2.455

Bae, C., R. Gnanasambandam, C. Nicolai, F. Sachs, and P.A. Gottlieb. 2013. Xerocytosis is caused by mutations that alter the kinetics of the mechanosensitive channel PIEZO1. *Proc. Natl. Acad. Sci. USA.* 110:E1162–E1168. https://doi.org/10.1073/pnas.1219777110

Bai, X., J. Bouffard, A. Lord, K. Brugman, P.W. Sternberg, E.J. Cram, and A. Golden. 2020. *Caenorhabditis elegans* PIEZO channel coordinates multiple reproductive tissues to govern ovulation. *eLife.* 9:e53603. https://doi.org/10.7554/eLife.53603

Ben Arous, J., S. Laffont, and D. Chatenay. 2009. Molecular and sensory basis of a food related two-state behavior in C. elegans. *PLoS One.* 4:e7584. https://doi.org/10.1371/journal.pone.0007584

Brenner, S. 1974. The genetics of Caenorhabditis elegans. *Genetics.* 77:71–94. https://doi.org/10.1093/genetics/77.1.71

Caires, R., F.J. Sierra-Valdez, J.R.M. Millet, J.D. Herwig, E. Roan, V. Vásquez, and J.F. Cordero-Morales. 2017. Omega-3 Fatty Acids Modulate TRPV4 Function through Plasma Membrane Remodeling. *Cell Rep.* 21:246–258. https://doi.org/10.1016/j.celrep.2017.09.029

Caires, R., B. Bell, J. Lee, L.O. Romero, V. Vásquez, and J.F. Cordero-Morales. 2021. Deficiency of Inositol Monophosphatase Activity Decreases Phosphoinositide Lipids and Enhances TRPV1 Function *In Vivo*. *J. Neurosci.* 41:408–423. https://doi.org/10.1523/JNEUROSCI.0803-20.2020

Chesler, A.T., M. Szczot, D. Bharucha-Goebel, M. Čeko, S. Donkervoort, C. Laubacher, L.H. Hayes, K. Alter, C. Zampieri, C. Stanley, et al. 2016. The Role of PIEZO2 in Human Mechanosensation. *N. Engl. J. Med.* 375:1355–1364. https://doi.org/10.1056/NEJMoa1602812

Coste, B. 2012. [Piezo proteins form a new class of mechanically activated ion channels]. *Med. Sci. (Paris).* 28:1056–1057. https://doi.org/10.1051/medsci/20122812012

Coste, B., J. Mathur, M. Schmidt, T.J. Earley, S. Ranade, M.J. Petrus, A.E. Dubin, and A. Patapoutian. 2010. Piezo1 and Piezo2 are essential components of distinct mechanically activated cation channels. *Science.* 330:55–60. https://doi.org/10.1126/science.1193270

Coste, B., G. Houge, M.F. Murray, N. Stitziel, M. Bandell, M.A. Giovanni, A. Philippakis, A. Hoischen, G. Riemer, U. Steen, et al. 2013. Gain-of-function mutations in the mechanically activated ion channel PIEZO2 cause a subtype of Distal Arthrogryposis. *Proc. Natl. Acad. Sci. USA.* 110:4667–4672. https://doi.org/10.1073/pnas.1221400110

Cox, C.D., N. Bavi, and B. Martinac. 2019. Biophysical Principles of Ion-Channel-Mediated Mechanosensory Transduction. *Cell Rep.* 29:1–12. https://doi.org/10.1016/j.celrep.2019.08.075

Dent, J.A., M.W. Davis, and L. Avery. 1997. avr-15 encodes a chloride channel subunit that mediates inhibitory glutamatergic neurotransmission and ivermectin sensitivity in Caenorhabditis elegans. *EMBO J.* 16:5867–5879. https://doi.org/10.1093/emboj/16.19.5867

Douguet, D., and E. Honoré. 2019. Mammalian Mechanoelectrical Transduction: Structure and Function of Force-Gated Ion Channels. *Cell.* 179:340–354. https://doi.org/10.1016/j.cell.2019.08.049

Fang-Yen, C., L. Avery, and A.D. Samuel. 2009. Two size-selective mechanisms specifically trap bacteria-sized food particles in Caenorhabditis elegans. *Proc. Natl. Acad. Sci. USA.* 106:20093–20096. https://doi.org/10.1073/pnas.0904036106

Ge, J., W. Li, Q. Zhao, N. Li, M. Chen, P. Zhi, R. Li, N. Gao, B. Xiao, and M. Yang. 2015. Architecture of the mammalian mechanosensitive Piezo1 channel. *Nature.* 527:64–69. https://doi.org/10.1038/nature15247

Geffeney, S.L., and M.B. Goodman. 2012. How we feel: ion channel partnerships that detect mechanical inputs and give rise to touch and pain perception. *Neuron.* 74:609–619. https://doi.org/10.1016/j.neuron.2012.04.023

Geron, M., R. Kumar, W. Zhou, J.D. Faraldo-Gómez, V. Vásquez, and A. Priel. 2018. TRPV1 pore turret dictates distinct DkTx and capsaicin gating. *Proc. Natl. Acad. Sci. USA.* 115:E11837–E11846. https://doi.org/10.1073/pnas.1809662115

Gottlieb, P.A., C. Bae, and F. Sachs. 2012. Gating the mechanical channel Piezo1: a comparison between whole-cell and patch recording. *Channels (Austin).* 6:282–289. https://doi.org/10.4161/chan.21064

Gruninger, T.R., D.G. Gualberto, and L.R. Garcia. 2008. Sensory perception of food and insulin-like signals influence seizure susceptibility. *PLoS Genet.* 4:e1000117. https://doi.org/10.1371/journal.pgen.1000117

Guo, Y.R., and R. MacKinnon. 2017. Structure-based membrane dome mechanism for Piezo mechanosensitivity. *eLife.* 6:e33660. https://doi.org/10.7554/eLife.33660

Hamilton, E.S., A.M. Schlegel, and E.S. Haswell. 2015. United in diversity: mechanosensitive ion channels in plants. *Annu. Rev. Plant Biol.* 66:113–137. https://doi.org/10.1146/annurev-arplant-043014-114700

Hardie, R.C. 2001. Phototransduction in Drosophila melanogaster. *J. Exp. Biol.* 204:3403–3409. https://doi.org/10.1242/jeb.204.20.3403

Hart, S.L., L.M. Boylan, S.R. Carroll, Y.A. Musick, C. Kuratko, B.G. Border, and R.M. Lampe. 2006. Brief report: newborn behavior differs with docosahexaenoic acid levels in breast milk. *J. Pediatr. Psychol.* 31:221–226 http://www.wormbook.org/chapters/www_behavior/behavior.html. https://doi.org/10.1093/jpepsy/jsj069

Hasse, S., A.A. Hyman, and M. Sarov. 2016. TransgeneOmics--A transgenic platform for protein localization based function exploration. *Methods.* 96:69–74. https://doi.org/10.1016/j.ymeth.2015.10.005

Höflich, J., P. Berninsone, C. Göbel, M.J. Gravato-Nobre, B.J. Libby, C. Darby, S.M. Politz, J. Hodgkin, C.B. Hirschberg, and R. Baumeister. 2004. Loss of srf-3-encoded nucleotide sugar transporter activity in Caenorhabditis elegans alters surface antigenicity and prevents bacterial adherence. *J. Biol. Chem.* 279:30440–30448. https://doi.org/10.1074/jbc.M402429200

Hou, S., Z. Jia, K. Kryszczuk, D. Chen, L. Wang, R. Holyst, and X. Feng. 2020. Joint effect of surfactants and cephalexin on the formation of Escherichia coli filament. *Ecotoxicol. Environ. Saf.* 199:110750. https://doi.org/10.1016/j.ecoenv.2020.110750

Hughes, K., A. Shah, X. Bai, J. Adams, R. Bauer, J. Jackson, E. Harris, A. Ficca, P. Freebairn, S. Mohammed, et al. 2021. Distinct mechanoreceptor *pezo-1* isoforms modulate food intake in the nematode *Caenorhabditis elegans*. *bioRxiv*. https://doi.org/10.1101/2021.05.24.445504

Ikeda, R., M. Cha, J. Ling, Z. Jia, D. Coyle, and J.G. Gu. 2014. Merkel cells transduce and encode tactile stimuli to drive Aβ-afferent impulses. *Cell.* 157:664–675. https://doi.org/10.1016/j.cell.2014.02.026

Jang, H., and C.I. Bargmann. 2013. Acute behavioral responses to pheromones in C. elegans (adult behaviors: attraction, repulsion). *Methods Mol. Biol.* 1068:285–292. https://doi.org/10.1007/978-1-62703-619-1_21

Keane, J., and L. Avery. 2003. Mechanosensory inputs influence Caenorhabditis elegans pharyngeal activity via ivermectin sensitivity genes. *Genetics.* 164:153–162. https://doi.org/10.1093/genetics/164.1.153

Kim, S.E., B. Coste, A. Chadha, B. Cook, and A. Patapoutian. 2012. The role of Drosophila Piezo in mechanical nociception. *Nature.* 483:209–212. https://doi.org/10.1038/nature10801

Kiyama, Y., K. Miyahara, and Y. Ohshima. 2012. Active uptake of artificial particles in the nematode Caenorhabditis elegans. *J. Exp. Biol.* 215:1178–1183. https://doi.org/10.1242/jeb.067199

Kung, C., B. Martinac, and S. Sukharev. 2010. Mechanosensitive channels in microbes. *Annu. Rev. Microbiol.* 64:313–329. https://doi.org/10.1146/annurev.micro.112408.134106

Lee, R.Y., E.R. Sawin, M. Chalfie, H.R. Horvitz, and L. Avery. 1999. EAT-4, a homolog of a mammalian sodium-dependent inorganic phosphate cotransporter, is necessary for glutamatergic neurotransmission in caenorhabditis elegans. *J. Neurosci.* 19:159–167. https://doi.org/10.1523/JNEUROSCI.19-01-00159.1999

Lee, K.S., S. Iwanir, R.B. Kopito, M. Scholz, J.A. Calarco, D. Biron, and E. Levine. 2017. Serotonin-dependent kinetics of feeding bursts underlie a graded response to food availability in C. elegans. *Nat. Commun.* 8:14221. https://doi.org/10.1038/ncomms14221

Li, Z., Y. Li, Y. Yi, W. Huang, S. Yang, W. Niu, L. Zhang, Z. Xu, A. Qu, Z. Wu, and T. Xu. 2012. Dissecting a central flip-flop circuit that integrates contradictory sensory cues in C. elegans feeding regulation. *Nat. Commun.* 3:776. https://doi.org/10.1038/ncomms1780

Li, J., B. Hou, S. Tumova, K. Muraki, A. Bruns, M.J. Ludlow, A. Sedo, A.J. Hyman, L. McKeown, R.S. Young, et al. 2014. Piezo1 integration of vascular architecture with physiological force. *Nature.* 515:279–282. https://doi.org/10.1038/nature13701

Ma, S., S. Cahalan, G. LaMonte, N.D. Grubaugh, W. Zeng, S.E. Murthy, E. Paytas, R. Gamini, V. Lukacs, T. Whitwam, et al. 2018. Common PIEZO1 Allele in African Populations Causes RBC Dehydration and Attenuates Plasmodium Infection. *Cell.* 173:443–455.e12. https://doi.org/10.1016/j.cell.2018.02.047

Maksimovic, S., M. Nakatani, Y. Baba, A.M. Nelson, K.L. Marshall, S.A. Wellnitz, P. Firozi, S.H. Woo, S. Ranade, A. Patapoutian, and E.A. Lumpkin. 2014. Epidermal Merkel cells are mechanosensory cells that tune mammalian touch receptors. *Nature.* 509:617–621. https://doi.org/10.1038/nature13250

Mango, S.E. 2007. The C. elegans pharynx: a model for organogenesis. *WormBook.*:1–26 http://www.wormbook.org/chapters/www_organformation/organformation.html. https://doi.org/10.1895/wormbook.1.129.1

Martinac, B., M. Buechner, A.H. Delcour, J. Adler, and C. Kung. 1987. Pressure-sensitive ion channel in Escherichia coli. *Proc. Natl. Acad. Sci. USA.* 84:2297–2301. https://doi.org/10.1073/pnas.84.8.2297

McMillin, M.J., A.E. Beck, J.X. Chong, K.M. Shively, K.J. Buckingham, H.I. Gildersleeve, M.I. Aracena, A.S. Aylsworth, P. Bitoun, J.C. Carey, et al. University of Washington Center for Mendelian Genomics. 2014. Mutations in PIEZO2 cause Gordon syndrome, Marden-Walker syndrome, and distal arthrogryposis type 5. *Am. J. Hum. Genet.* 94:734–744. https://doi.org/10.1016/j.ajhg.2014.03.015

Min, S., Y. Oh, P. Verma, S.C. Whitehead, N. Yapici, D. Van Vactor, G.S. Suh, and S. Liberles. 2021. Control of feeding by Piezo-mediated gut mechanosensation in *Drosophila*. *eLife.* 10:e63049. https://doi.org/10.7554/eLife.63049

Murthy, S.E., M.C. Loud, I. Daou, K.L. Marshall, F. Schwaller, J. Kühnemund, A.G. Francisco, W.T. Keenan, A.E. Dubin, G.R. Lewin, and A. Patapoutian. 2018. The mechanosensitive ion channel Piezo2 mediates sensitivity to mechanical pain in mice. *Sci. Transl. Med.* 10:eaat9897. https://doi.org/10.1126/scitranslmed.aat9897

Niacaris, T., and L. Avery. 2003. Serotonin regulates repolarization of the C. elegans pharyngeal muscle. *J. Exp. Biol.* 206:223–231. https://doi.org/10.1242/jeb.00101

Ohmachi, M., A. Sugimoto, Y. Iino, and M. Yamamoto. 1999. kel-1, a novel Kelch-related gene in Caenorhabditis elegans, is expressed in pharyngeal gland cells and is required for the feeding process. *Genes Cells.* 4:325–337. https://doi.org/10.1046/j.1365-2443.1999.00264.x

Pan, B., N. Akyuz, X.P. Liu, Y. Asai, C. Nist-Lund, K. Kurima, B.H. Derfler, B. György, W. Limapichat, S. Walujkar, et al. 2018. TMC1 Forms the Pore of Mechanosensory Transduction Channels in Vertebrate Inner Ear Hair Cells. *Neuron.* 99:736–753.e6. https://doi.org/10.1016/j.neuron.2018.07.033

Parpaite, T., and B. Coste. 2017. Piezo channels. *Curr. Biol.* 27:R250–R252. https://doi.org/10.1016/j.cub.2017.01.048

Pathak, M.M., J.L. Nourse, T. Tran, J. Hwe, J. Arulmoli, D.T. Le, E. Bernardis, L.A. Flanagan, and F. Tombola. 2014. Stretch-activated ion channel Piezo1 directs lineage choice in human neural stem cells. *Proc. Natl. Acad. Sci. USA.* 111:16148–16153. https://doi.org/10.1073/pnas.1409802111

Raizen, D.M., and L. Avery. 1994. Electrical activity and behavior in the pharynx of Caenorhabditis elegans. *Neuron.* 12:483–495. https://doi.org/10.1016/0896-6273(94)90207-0

Raizen, D.M., R.Y. Lee, and L. Avery. 1995. Interacting genes required for pharyngeal excitation by motor neuron MC in Caenorhabditis elegans. *Genetics.* 141:1365–1382. https://doi.org/10.1093/genetics/141.4.1365

Ranade, S.S., S.H. Woo, A.E. Dubin, R.A. Moshourab, C. Wetzel, M. Petrus, J. Mathur, V. Bégay, B. Coste, J. Mainquist, et al. 2014. Piezo2 is the major transducer of mechanical forces for touch sensation in mice. *Nature.* 516:121–125. https://doi.org/10.1038/nature13980

Retailleau, K., F. Duprat, M. Arhatte, S.S. Ranade, R. Peyronnet, J.R. Martins, M. Jodar, C. Moro, S. Offermanns, Y. Feng, et al. 2015. Piezo1 in Smooth Muscle Cells Is Involved in Hypertension-Dependent Arterial Remodeling. *Cell Rep.* 13:1161–1171. https://doi.org/10.1016/j.celrep.2015.09.072

Rode, B., J. Shi, N. Endesh, M.J. Drinkhill, P.J. Webster, S.J. Lotteau, M.A. Bailey, N.Y. Yuldasheva, M.J. Ludlow, R.M. Cubbon, et al. 2017. Piezo1 channels sense whole body physical activity to reset cardiovascular homeostasis and enhance performance. *Nat. Commun.* 8:350. https://doi.org/10.1038/s41467-017-00429-3

Romero, L.O., A.E. Massey, A.D. Mata-Daboin, F.J. Sierra-Valdez, S.C. Chauhan, J.F. Cordero-Morales, and V. Vásquez. 2019. Dietary fatty acids fine-tune Piezo1 mechanical response. *Nat. Commun.* 10:1200. https://doi.org/10.1038/s41467-019-09055-7

Saotome, K., S.E. Murthy, J.M. Kefauver, T. Whitwam, A. Patapoutian, and A.B. Ward. 2018. Structure of the mechanically activated ion channel Piezo1. *Nature.* 554:481–486. https://doi.org/10.1038/nature25453

Schindelin, J., I. Arganda-Carreras, E. Frise, V. Kaynig, M. Longair, T. Pietzsch, S. Preibisch, C. Rueden, S. Saalfeld, B. Schmid, et al. 2012. Fiji: an open-source platform for biological-image analysis. *Nat. Methods.* 9:676–682. https://doi.org/10.1038/nmeth.2019

Schulenburg, H., and M.A. Félix. 2017. The Natural Biotic Environment of *Caenorhabditis elegans*. *Genetics.* 206:55–86. https://doi.org/10.1534/genetics.116.195511

Shtonda, B.B., and L. Avery. 2006. Dietary choice behavior in Caenorhabditis elegans. *J. Exp. Biol.* 209:89–102. https://doi.org/10.1242/jeb.01955

Singh, R.N.S., and J.E. Sulston. 1978. Some Observations On Moulting in Caenorhabditis Elegans. *Nematologica.* 24:63–71. https://doi.org/10.1163/187529278X00074

Smit, R.B., R. Schnabel, and J. Gaudet. 2008. The HLH-6 transcription factor regulates C. elegans pharyngeal gland development and function. *PLoS Genet.* 4:e1000222. https://doi.org/10.1371/journal.pgen.1000222

Strange, K., M. Christensen, and R. Morrison. 2007. Primary culture of Caenorhabditis elegans developing embryo cells for electrophysiological,

cell biological and molecular studies. *Nat. Protoc.* 2:1003–1012. https://doi.org/10.1038/nprot.2007.143

Szczot, M., J. Liljencrantz, N. Ghitani, A. Barik, R. Lam, J.H. Thompson, D. Bharucha-Goebel, D. Saade, A. Necaise, S. Donkervoort, et al. 2018. PIEZO2 mediates injury-induced tactile pain in mice and humans. *Sci. Transl. Med.* 10:eaat9892. https://doi.org/10.1126/scitranslmed.aat9892

Taylor, S.R., G. Santpere, A. Weinreb, A. Barrett, M.B. Reilly, C. Xu, E. Varol, P. Oikonomou, L. Glenwinkel, R. McWhirter, et al. 2021. Molecular topography of an entire nervous system. *Cell.* 184:4329–4347.e23. https://doi.org/10.1016/j.cell.2021.06.023

Trojanowski, N.F., D.M. Raizen, and C. Fang-Yen. 2016. Pharyngeal pumping in Caenorhabditis elegans depends on tonic and phasic signaling from the nervous system. *Sci. Rep.* 6:22940. https://doi.org/10.1038/srep22940

Tsujimura, T., R. Ueha, M. Yoshihara, E. Takei, K. Nagoya, N. Shiraishi, J. Magara, and M. Inoue. 2019. Involvement of the epithelial sodium channel in initiation of mechanically evoked swallows in anaesthetized rats. *J. Physiol.* 597:2949–2963. https://doi.org/10.1113/JP277895

Van Gilst, M.R., H. Hadjivassiliou, A. Jolly, and K.R. Yamamoto. 2005. Nuclear hormone receptor NHR-49 controls fat consumption and fatty acid composition in C. elegans. *PLoS Biol.* 3:e53. https://doi.org/10.1371/journal.pbio.0030053

Vidal-Gadea, A.G., S. Davis, L. Becker, and J.T. Pierce-Shimomura. 2012. Coordination of behavioral hierarchies during environmental transitions in *Caenorhabditis elegans*. *Worm.* 1:5–11. https://doi.org/10.4161/worm.19148

Wang, S., R. Chennupati, H. Kaur, A. Iring, N. Wettschureck, and S. Offermanns. 2016. Endothelial cation channel PIEZO1 controls blood pressure by mediating flow-induced ATP release. *J. Clin. Invest.* 126:4527–4536. https://doi.org/10.1172/JCI87343

Wang, P., Y. Jia, T. Liu, Y.N. Jan, and W. Zhang. 2020. Visceral Mechanosensing Neurons Control Drosophila Feeding by Using Piezo as a Sensor. *Neuron.* 108:640–650.e4. https://doi.org/10.1016/j.neuron.2020.08.017

Woo, S.H., S. Ranade, A.D. Weyer, A.E. Dubin, Y. Baba, Z. Qiu, M. Petrus, T. Miyamoto, K. Reddy, E.A. Lumpkin, et al. 2014. Piezo2 is required for Merkel-cell mechanotransduction. *Nature.* 509:622–626. https://doi.org/10.1038/nature13251

Woo, S.H., V. Lukacs, J.C. de Nooij, D. Zaytseva, C.R. Criddle, A. Francisco, T.M. Jessell, K.A. Wilkinson, and A. Patapoutian. 2015. Piezo2 is the principal mechanotransduction channel for proprioception. *Nat. Neurosci.* 18:1756–1762. https://doi.org/10.1038/nn.4162

Wu, J., A.H. Lewis, and J. Grandl. 2017a. Touch, Tension, and Transduction - The Function and Regulation of Piezo Ion Channels. *Trends Biochem. Sci.* 42:57–71. https://doi.org/10.1016/j.tibs.2016.09.004

Wu, J., M. Young, A.H. Lewis, A.N. Martfeld, B. Kalmeta, and J. Grandl. 2017b. Inactivation of Mechanically Activated Piezo1 Ion Channels Is Determined by the C-Terminal Extracellular Domain and the Inner Pore Helix. *Cell Rep.* 21:2357–2366. https://doi.org/10.1016/j.celrep.2017.10.120

Yamaguchi, T., K. Takano, Y. Inaba, M. Morikawa, M. Motobayashi, R. Kawamura, K. Wakui, E. Nishi, S.I. Hirabayashi, Y. Fukushima, et al. 2019. PIEZO2 deficiency is a recognizable arthrogryposis syndrome: A new case and literature review. *Am. J. Med. Genet. A.* 179:948–957. https://doi.org/10.1002/ajmg.a.61142

Yan, Z., W. Zhang, Y. He, D. Gorczyca, Y. Xiang, L.E. Cheng, S. Meltzer, L.Y. Jan, and Y.N. Jan. 2013. Drosophila NOMPC is a mechanotransduction channel subunit for gentle-touch sensation. *Nature.* 493:221–225. https://doi.org/10.1038/nature11685

Yu, L., X. Yan, C. Ye, H. Zhao, X. Chen, F. Hu, and H. Li. 2015. Bacterial Respiration and Growth Rates Affect the Feeding Preferences, Brood Size and Lifespan of Caenorhabditis elegans. *PLoS One.* 10:e0134401. https://doi.org/10.1371/journal.pone.0134401

Zarychanski, R., V.P. Schulz, B.L. Houston, Y. Maksimova, D.S. Houston, B. Smith, J. Rinehart, and P.G. Gallagher. 2012. Mutations in the mechanotransduction protein PIEZO1 are associated with hereditary xerocytosis. *Blood.* 120:1908–1915. https://doi.org/10.1182/blood-2012-04-422253

Zeng, W.Z., K.L. Marshall, S. Min, I. Daou, M.W. Chapleau, F.M. Abboud, S.D. Liberles, and A. Patapoutian. 2018. PIEZOs mediate neuronal sensing of blood pressure and the baroreceptor reflex. *Science.* 362:464–467. https://doi.org/10.1126/science.aau6324

Zhao, Q., H. Zhou, S. Chi, Y. Wang, J. Wang, J. Geng, K. Wu, W. Liu, T. Zhang, M.Q. Dong, et al. 2018. Structure and mechanogating mechanism of the Piezo1 channel. *Nature.* 554:487–492. https://doi.org/10.1038/nature25743

Supplemental material

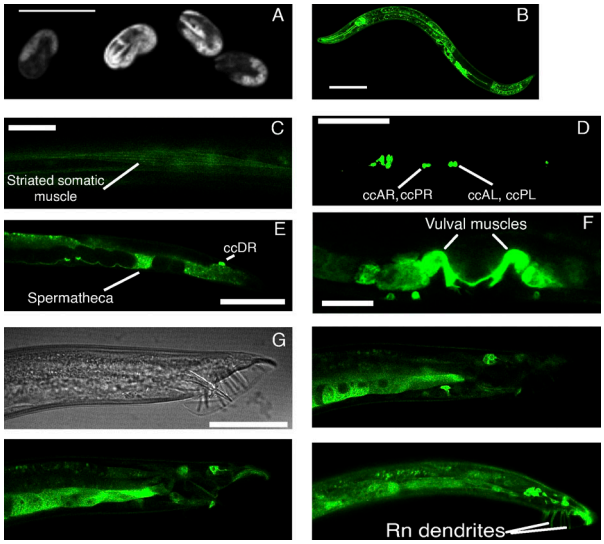

Figure S1. ***pezo-1* is expressed in a variety of tissues in *C. elegans*. (A)** Micrograph of *pezo-1::GFP* eggs. Scale bar represents 50 µm. **(B)** Micrograph of an L4 *pezo-1::GFP* hermaphrodite expressing GFP. Scale bar represents 100 µm. **(C)** Micrograph of a young adult *pezo-1::GFP* hermaphrodite expressing GFP in somatic muscles located in the anterior end of the animal. Scale bar represents 20 µm. **(D)** Micrograph of a young adult *pezo-1::GFP* hermaphrodite expressing GFP in the coelomocytes (ccAR, ccAL, ccPL). Scale bar represents 100 µm. **(E)** Micrograph of a larval *pezo-1::GFP* hermaphrodite expressing GFP in the spermatheca and in coelomocyte ccDR. Scale bar represents 100 µm. **(F)** Micrograph of a young adult *pezo-1::GFP* hermaphrodite expressing GFP in the vulval muscle. Scale bar represents 20 µm. **(G)** Micrographs (4) of a *pezo-1::GFP* adult male expressing GFP in the tail. Scale bar represents 50 µm. Rn, ray neuron.

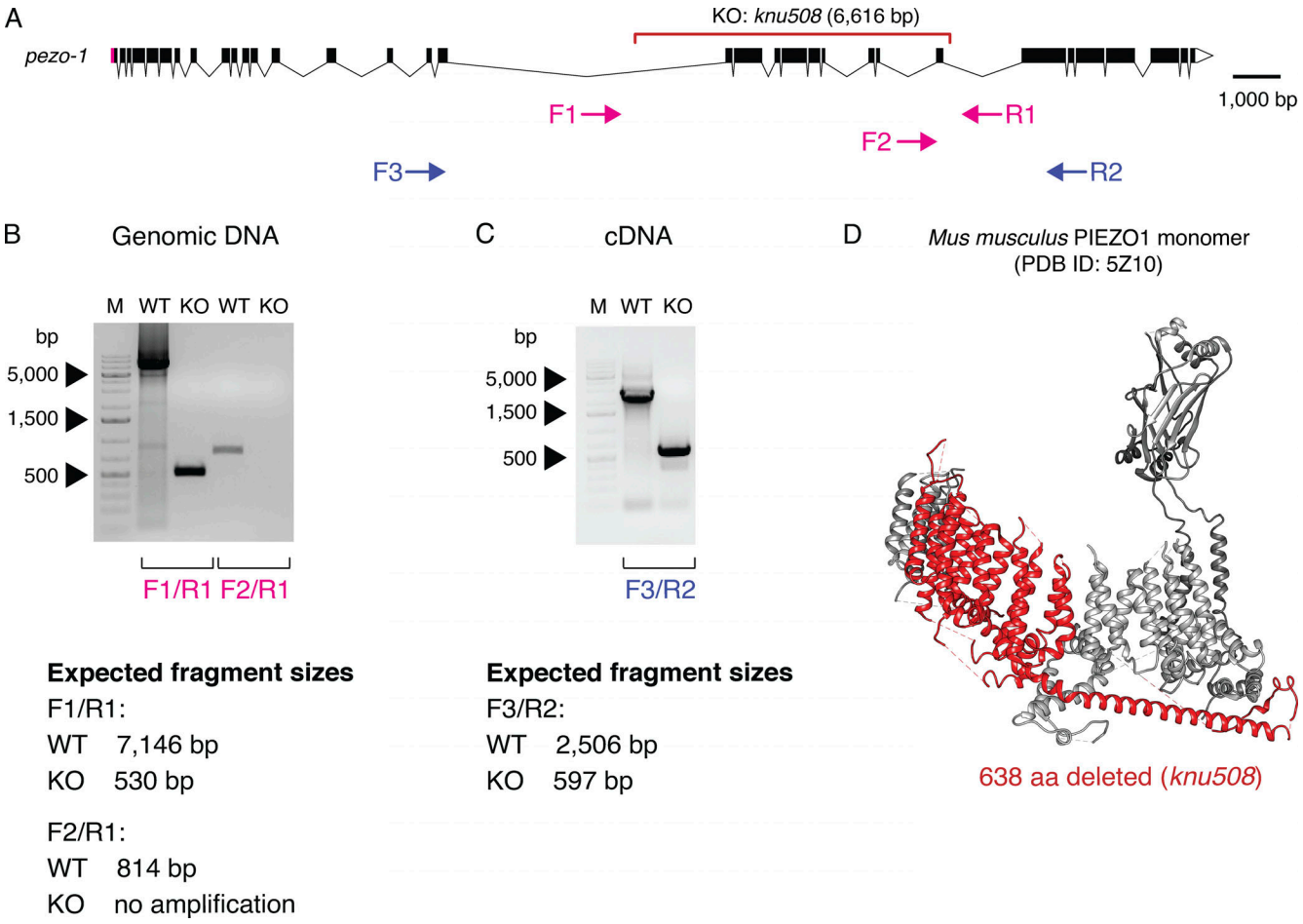

Figure S2. ***pezo-1* KO validation. (A)** *pezo-1* gene diagram according to wormbase.org release WS280 made with Exon-Intron Graphic Maker (wormweb.org). Magenta rectangles and white triangles denote the 5′ and 3′ UTRs, respectively; black rectangles denote exons; black lines denote introns; the red bracket denotes the *knu508* allele (a 6,616-bp deletion) of the *pezo-1* KO strain; magenta arrows labeled F1, F2, and R1 denote the positions of the oligonucleotides used for PCR amplification; and blue arrows F3 and R2 denote the positions of the oligonucleotides used for RT-PCR amplification. **(B)** Agarose gel electrophoresis (1% agarose) of PCR-amplified products using F1/R1 and F2/R1 PCR primer sets. Lane M, 1 kb Plus DNA (SM1331/2; Thermo Fisher Scientific) size marker. WT (N2) and KO (COP1553) refer to the worm strains used to extract genomic DNA. **(C)** Agarose gel electrophoresis (1% agarose) of RT-PCR amplified products using F3/R2 primer sets. Lane M, 1 kb Plus DNA (SM1331/2; Thermo Fisher Scientific) size marker. WT (N2) and KO (COP1553) refer to the worm strains used to extract total RNA. **(D)** Ribbon representation of *Mus musculus* PIEZO1 monomer (PDB ID: 5Z10; gray) highlighting the PEZO-1 corresponding residues (red) that were knocked out using CRISPR to generate the *knu508* allele. PEZO-1 monomer ribbon diagram was made with UCSF Chimera v1.9.

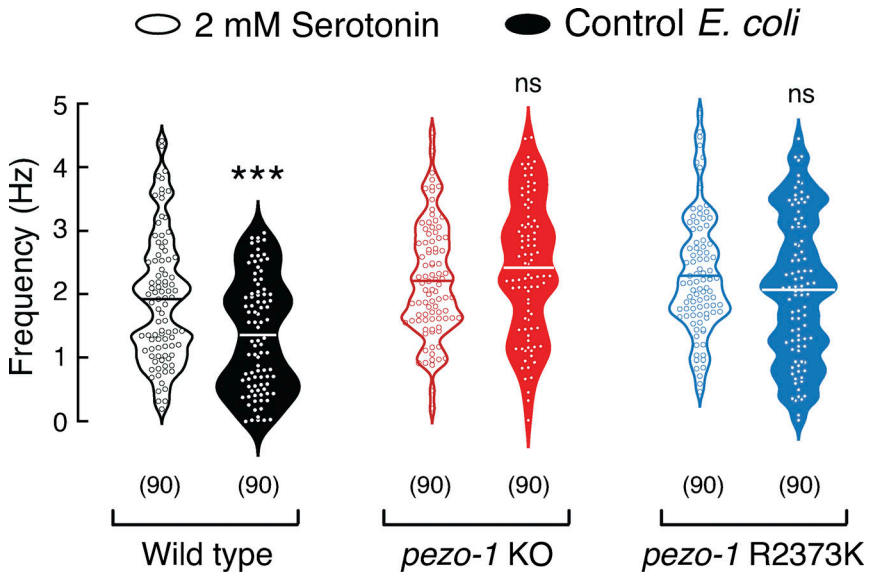

Figure S3. **Comparison between *pezo-1* strains pumping frequencies elicited by serotonin or bacteria.** Pharyngeal pumping frequencies depicted as violin plots with the means shown as horizontal bars, for WT (N2), *pezo-1* KO, and *pezo-1* R2373K strains at 2 mM serotonin concentration or when fed with control *E. coli*. *n* is denoted above the x axis. Mann–Whitney test. Asterisks indicate values that are significantly different (***, P < 0.001), and ns indicates not significantly different.

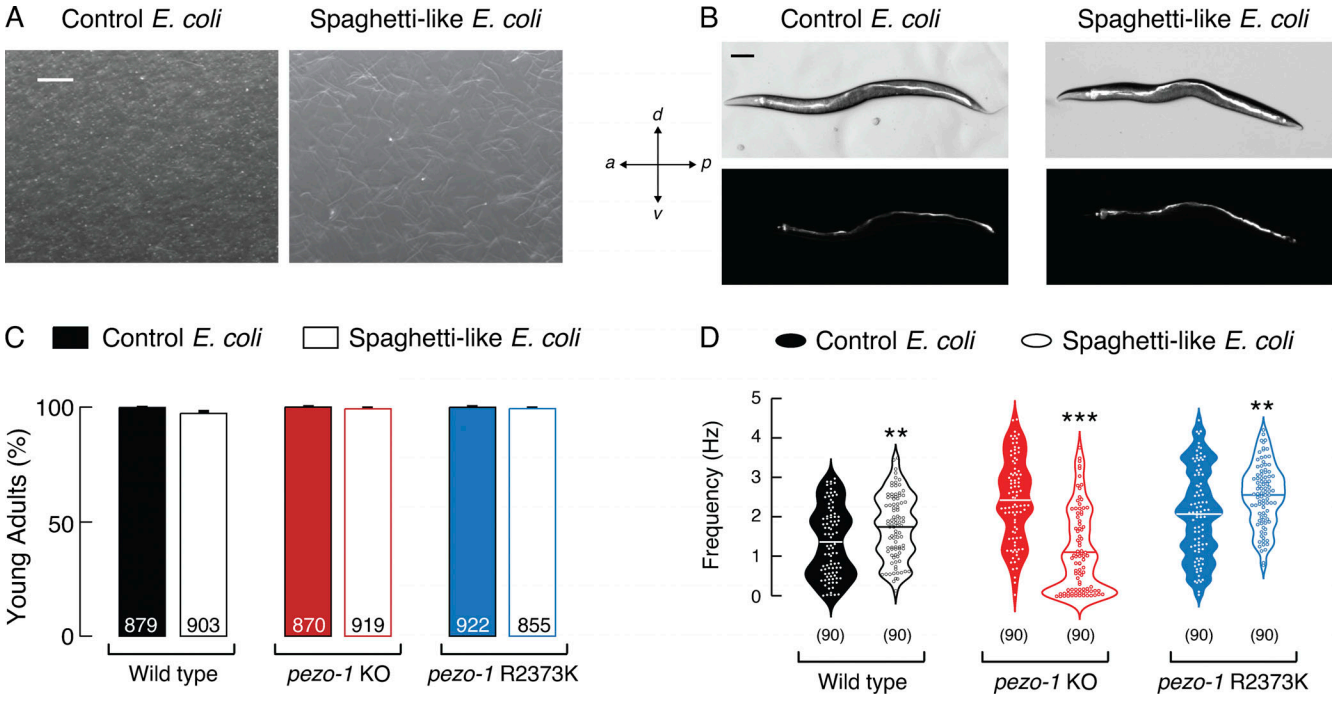

Figure S4. **Worms eat spaghetti-like bacteria and reach adulthood. (A)** Representative micrographs of control (left) and cephalexin-treated (right; spaghetti-like) *E. coli* cultures. Scale bar represents 200 µm. **(B)** Representative micrographs of adult worms fed with control (left) and cephalexin-treated (right; spaghetti-like) *E. coli* dyed with 2 µM DiI. Scale bar represents 100 µm. **(C)** WT (N2), *pezo-1* KO, and *pezo-1* R2373K adult proportion after 3 d of seeding eggs on NGM plates with control or spaghetti-like bacteria, as determined by worm images. Animals that reached adulthood were counted in each trial, and results were compared across four trials. *n* is denoted inside the bars. **(D)** Pharyngeal pumping frequencies depicted as violin plots with the means shown as horizontal bars, for WT (N2), *pezo-1* KO, and *pezo-1* R2373K strains when fed with control or cephalexin-treated *E. coli* (spaghetti-like bacteria). *n* is denoted above the x axis. Mann–Whitney test. Asterisks indicate values that are significantly different (***, P < 0.001 and **, P < 0.01), and ns indicates not significantly different.

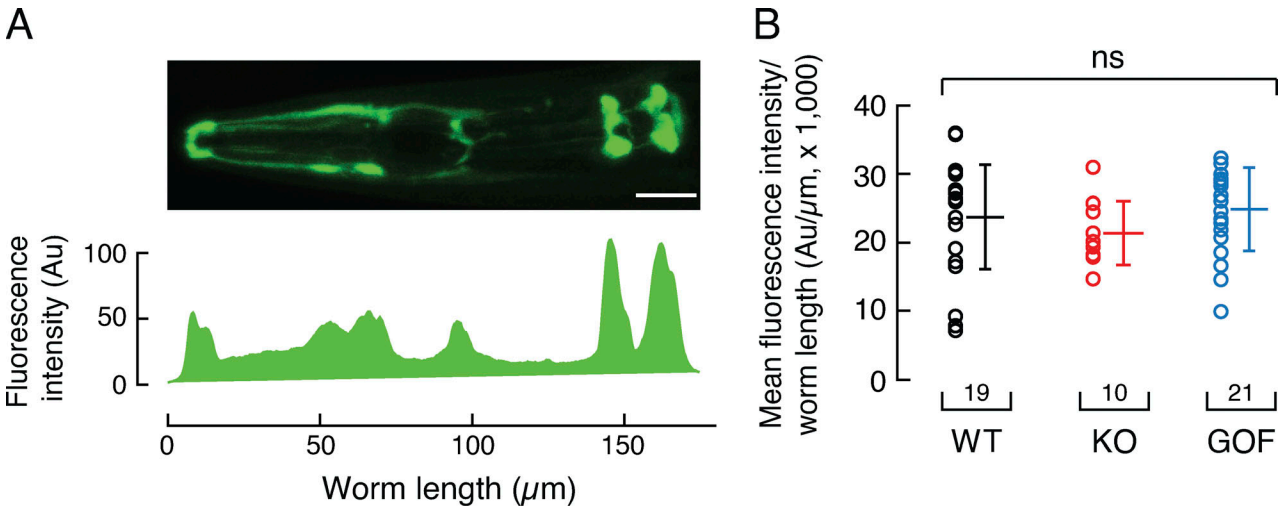

Figure S5. **Fluorescence intensity of cells expressing *pezo-1::GFP* from WT, *pezo*-1 KO, and *pezo-1* R2373K strains. (A)** Top: Representative fluorescence micrograph of the anterior end of a young adult *pezo-1::GFP* hermaphrodite highlighting the GFP reporter expression in pharynx structures and gland cells. Scale bar represents 20 µm. Bottom: Representative fluorescence intensity profile obtained from top micrograph. **(B)** Mean/scatter-dot plot representing the mean fluorescence intensity per worm length of *pezo-1::GFP* from WT, pezo-1 KO, and *pezo-1* R2373K strains. One-way ANOVA. *n* is denoted above the x axis. ns indicates not significantly different.

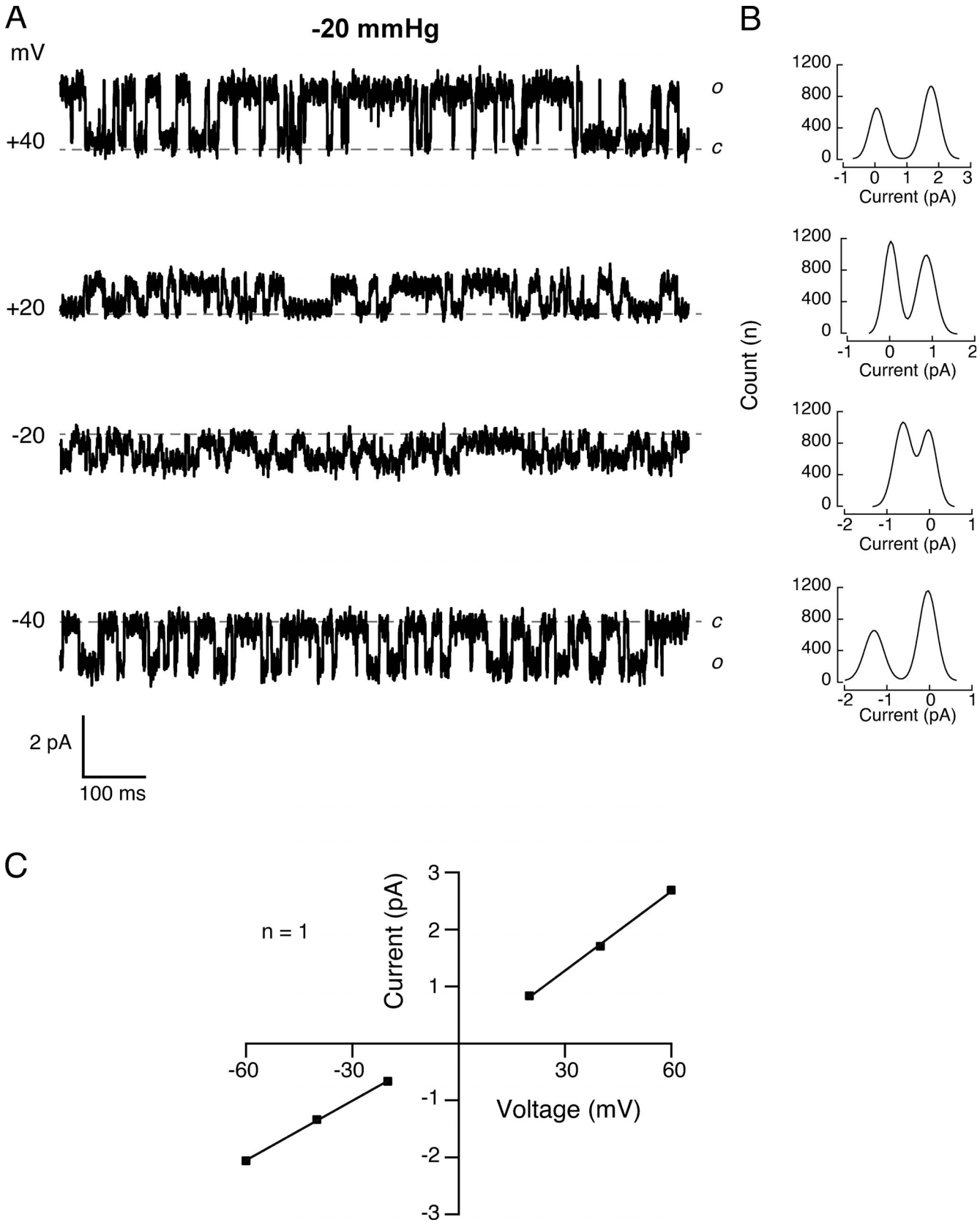

Figure S6. **Mechanosensitive channel currents of cells expressing *pezo-1::GFP*. (A)** Representative single-channel trace recordings of WT cells expressing *pezo-1::GFP* in the cell-attached configuration. Channel openings were elicited by −20 mmHg of negative pressure at constant voltages. Closed and open states are labeled *c* and *o*, respectively. **(B)** All-point amplitude histograms of pressure-evoked single-channel currents from recordings shown in A. **(C)** Current–voltage relationship at constant pressure (−20 mmHg). Outward slope conductance, 46.37 pS; inward slope conductance, 34.85 pS.

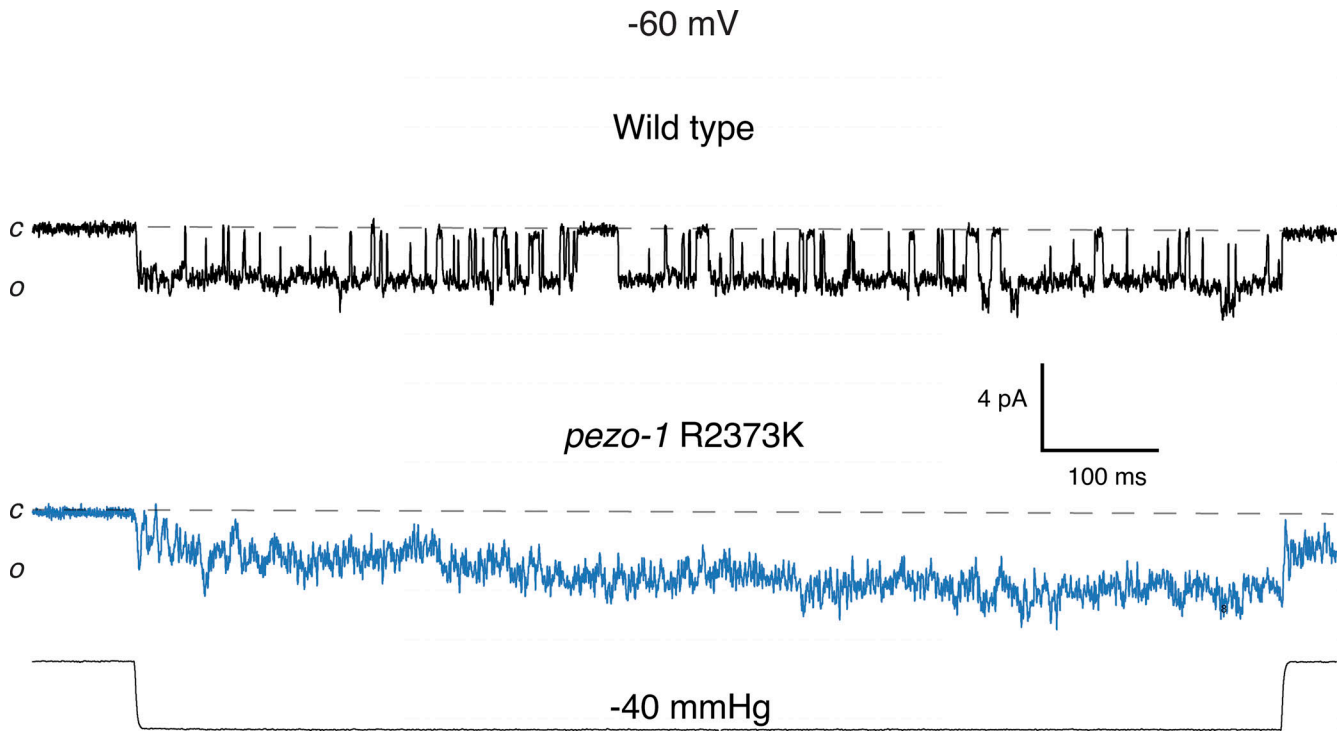

Figure S7. **Mechanosensitive channel traces of cells expressing *pezo-1::GFP*.** Representative single-channel trace recordings of pressure-evoked currents from *pezo-1::GFP* cells expressing *pezo-1* WT and R2373K, in the cell-attached configuration. Channel openings were elicited by −40 mmHg at a constant voltage of −60 mV. These are the same records shown in Fig. 7, A and B, used to generate the all-point amplitude histograms, filtered offline at 1 kHz to highlight single-channel events. Closed and open states are labeled *c* and *o*, respectively.

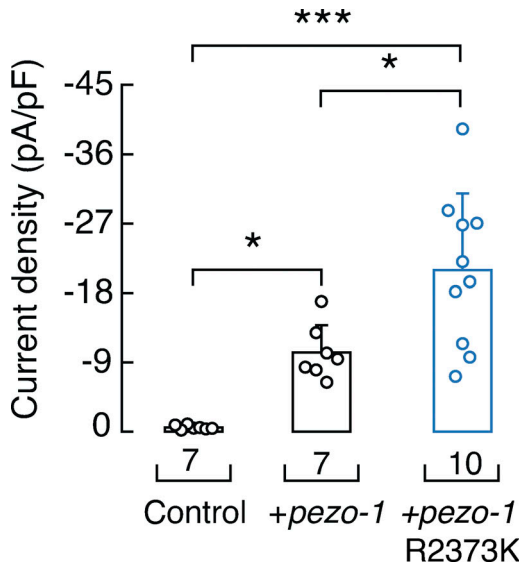

Figure S8. **PEZO-1 WT or R2373K current densities in Sf9 cells.** Current densities elicited by maximum displacement of Sf9 cells control (uninfected), expressing *pezo-1* WT or R2373K. *n* is denoted above the x axis. One-way ANOVA and Tukey–Kramer multiple comparisons test. Asterisks indicate values significantly different (***, P < 0.001 and *, P < 0.05).

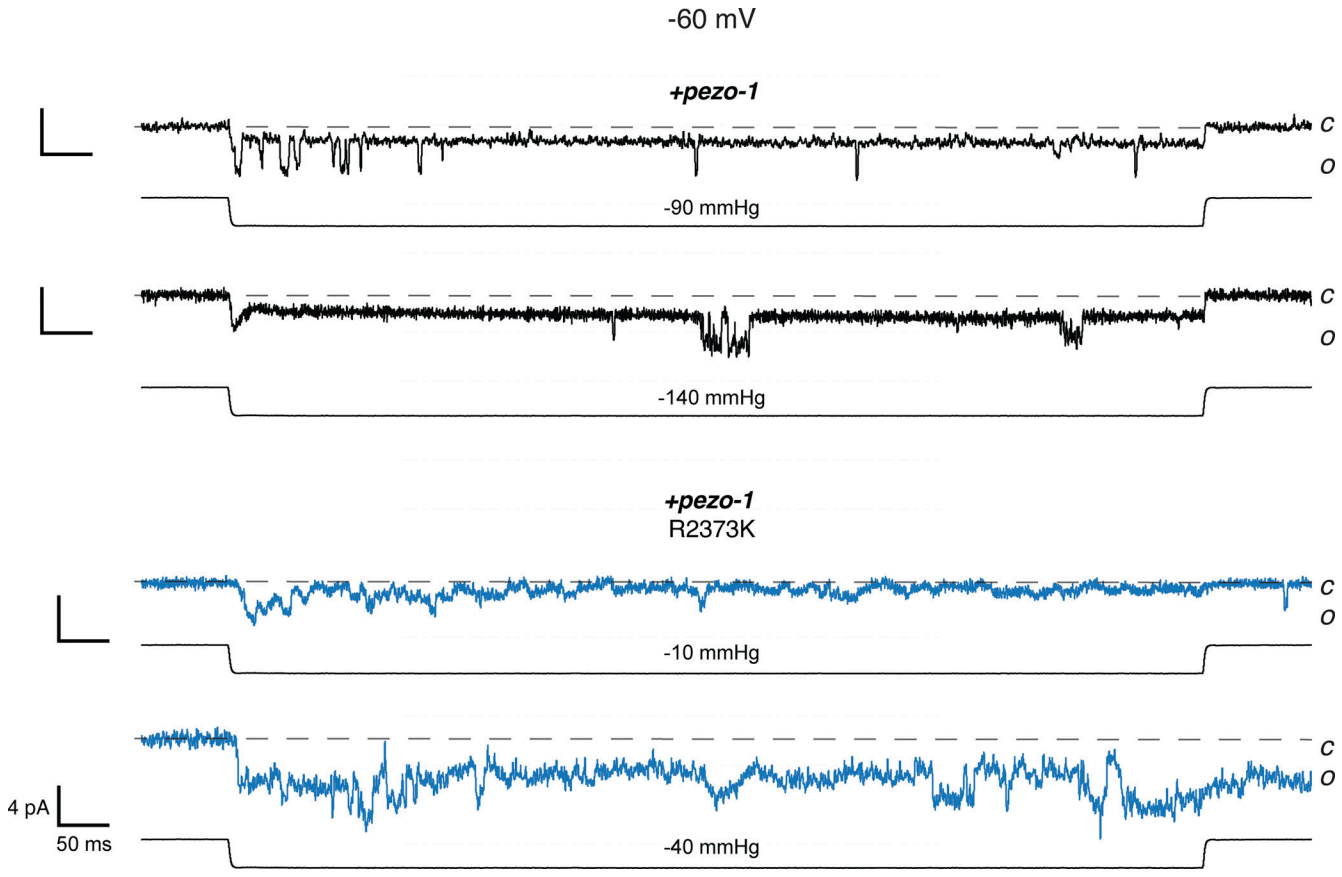

Figure S9. **Single-channel traces of pressure-evoked currents of PEZO-1 WT or R2373K in Sf9 cells.** Representative trace recordings of pressure-evoked currents from Sf9 cells expressing *pezo-1* WT or R2373K, recorded in the inside-out configuration. Channel openings were elicited by negative pressure at −60 mV. Traces were filtered offline at 1 kHz to highlight single-channel events. Closed and open states are labeled *c* and *o*, respectively.